Nonlinear Dyn
https://doi.org/10.1007/s11071-019-05373-z

ORIGINAL PAPER

Spectro-spatial analyses of a nonlinear metamaterial with multiple nonlinear local resonators

Mohammad Bukhari · Oumar Barry

Received: 3 May 2019 / Accepted: 14 November 2019

Abstract Recent focus has been given to spectro-spatial analysis of nonlinear metamaterials since they can predict interesting nonlinear phenomena not accessible by spectral analysis (i.e., dispersion relations). However, current studies are limited to a nonlinear chain with single linear resonator or linear chain with nonlinear resonator. There is no work that examines the combination of nonlinear chain with nonlinear resonators. This paper investigates the spectro-spatial properties of wave propagation through a nonlinear metamaterials consisting of nonlinear chain with multiple nonlinear local resonators. Different combinations of softening and hardening nonlinearities are examined to reveal their impact on the traveling wave features and the band structure. The method of multiple scales is used to obtain closed-form expressions for the dispersion relations. Our analytical solution is validated via the numerical simulation and results from the literature. The numerical simulation is based on spectro-spatial analysis using signal processing techniques such as spatial spectrogram, wave filtering, and contour plots of 2D Fourier transform. The spectro-spatial analysis provides a detailed information about wave distortion due to nonlinearity and classify the distortion into different features. The observations suggest that nonlinear chain with multiple nonlinear resonators can affect the waveform at all wavelength limits. Such nonlinear metamaterials are suitable for broadband vibration control and energy harvesting, as well as other applications such as acoustic switches, diodes, and rectifiers, allowing wave propagation only in a pre-defined direction.

Keywords Nonlinear metamaterial · Spectro-spatial analysis · Perturbation techniques · Dispersion relations · Solitary waves

M. Bukhari · O. Barry (✉)
Department of Mechanical Engineering, Virginia Tech, Blacksburg, Virginia 24061, USA
e-mail: obarry@vt.edu

1 Introduction

The study of metamaterials has gained lots of attention in recent years due to their exceptional material properties characteristics and their wider engineering applications. Metamaterials are a new class of artificial composites that derive their unique dynamic properties from both engineered local configurations and material constituents [1]. They were originally developed for electromagnetic and optical wave propagation, and later the technology was extended to acoustic and elastic waves [2]. Metamaterials can be constructed as periodic structures (i.e., phononic crystals in the presence or absence of local resonator) or in random arrangements (usually in the presence of local resonator). However, locally resonant metamaterials draw their interesting dynamic phenomena because of the presence of local resonators rather than periodicity [3]. These interesting dynamic features can be judiciously employed for suppressing noise and vibration, harvesting energy,

Published online: 26 November 2019

nondestructive testing structures for defects, improving image resolution, and ameliorating the performance of antennas and many other engineering structures and devices [4].

The study of periodic structures reveals the development of a frequency bandgap where the wave does not propagate through the structure, instead it gets reflected [5–10]. These frequencies are associated with wavelength near the size of lattice constant. The wave attenuation is caused by Bragg scattering and offers a good vibration control in low-frequency region. However, the restriction on the lattice size limits the advantage of Bragg scattering to large structures applications.

Due to the crucial need for extending these phenomena to control much smaller-size structures (e.g., MEMS), Liu et al. [11] suggested embedding smaller resonators inside crystals to form locally resonant metamaterials. Locally resonant metamaterials form a bandgap at wave lengths much larger than the lattice constant. Indeed, the bandgap formation results from the combination of Bragg scattering and local resonance when the frequency of the local resonator is not very low. Nevertheless, the parameters of the resonator govern the dominant effect of the bandgap formation [12]. Yet, very low-frequency local resonators can still be excited by long wavelength waves, and hence, bandgap can be formed due to hybridization of the local resonances only and without the need for Bragg scattering [3]. Controlling different frequency regions requires using different resonators inside the lattice [13,14], such that wave attenuation can be observed in the vicinity of different local resonances. Intentionally introducing nonlinearity can reveal additional interesting wave propagation phenomena which widens the applications of metamaterials. Some of those, but not limited to, are gap solitons [15], envelope and dark solitons [16], asymmetric wave propagation [17], and adjusting band structure limits [18].

Based on the magnitude of nonlinearity, the metamaterial can be classified as a strongly or weakly nonlinear. The latter may be asymptotically converging, and an explicit approximate solution can be presented by perturbation techniques [19,20]. For instance, dispersion relation of nonlinear chain (metamaterial) can be obtained by Lindstedt–Poincare method [21]. However, for more complicated or interacting nonlinear systems, the method of multiple scales is more convenient since the associated algebra requires much less effort [22,23]. Yet dispersion curves in nonlinear continuous metamaterials can be approximated by using the transfer matrix method [24]. Studying nonlinear dispersion curves can reveal important information about the effect of nonlinearity on the wave propagation (e.g., dispersive and solitary waves) [25].

Recent trends in nonlinear metamaterials focus on wave non-reciprocity such that unidirection wave propagation can be utilized to passively develop acoustic diodes, switches, and rectifiers. For example, acoustic diodes can be obtained by coupling nonlinear and linear chains [17,26,27]. This requires tuning the secondary resonances of nonlinear chain to the passband of a linear chain. For instance, exciting weakly nonlinear oscillator with cubic nonlinearity can develop a signal with subharmonic resonance. If this secondary resonance lies in the passband of coupled wave while the original excitation frequency lies in the bandgap, waves can only propagate in the direction from nonlinear to linear chain [28]. Similarly, bifurcation due to defects in granular chains can allow the wave to propagate only in one direction [29]. Nonlinear energy sink can also form wave non-reciprocity in hierarchical internal structures [30].

Nonlinear metamaterials are often analyzed by tracking the change in the temporal state properties and discussing the existence of solitary waves and dispersion characteristics. Dispersion relations do not, however, reveal enough detailed information on the wave distortion features. On the other hand, spectro-spatial analyses can provide better understanding of the physical features of wave propagation such as frequency shift and wave localization or dispersion in a nonlinear medium. Ganesh and Gonella [31] were the first to study the spectro-spatial wave packet propagation features of nonlinear periodic chains using signal processing tools to highlight new important nonlinear wave propagation properties. Their analysis provided more detailed information about the wave distribution such as conditions related to the birth or inhalation of solitary wave at different wavelengths. Their work was extended by Zhou et al. [32], who investigated the spectro-spatial features of nonlinear acoustic metamaterials consisting of nonlinear cell with a linear local resonator. Their study showed that nonlinearity gives rise to nondispersive features in wave propagation. The spectro-spatial features in [31,32] revealed that nonlinear phenomena affect only short wavelength domain. This is because the nonlinearity was limited to the springs connecting the cells only. None of the afore-

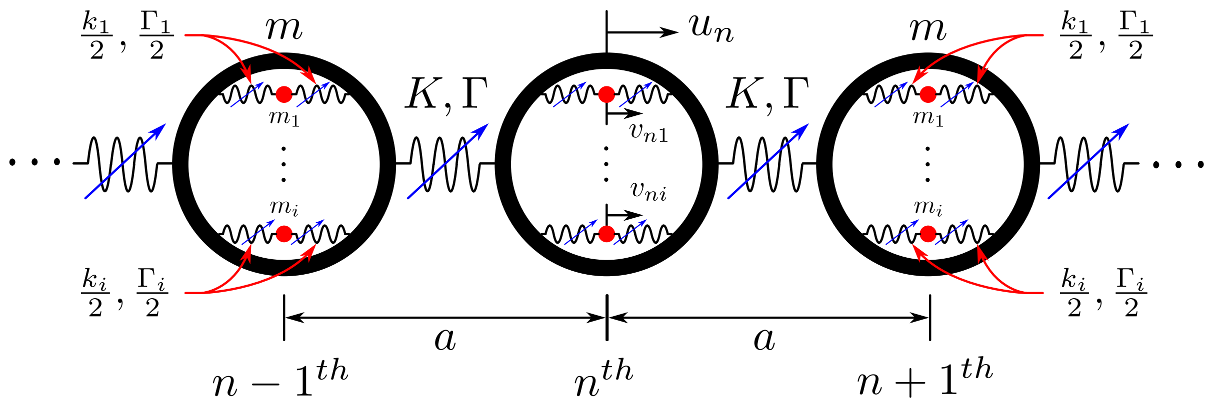

Fig. 1 Schematic diagram for the nonlinear acoustic metamaterials with nonlinear resonators

mentioned studies included nonlinearities in the local resonators. Recently, we presented for the first time the spectral analysis (i.e., dispersion relations only) of a nonlinear metamaterials consisting of nonlinear (or linear) chain with linear (or nonlinear) multiple local resonators [33]. Our work indicated that the dispersion relations for nonlinear chain with linear resonator and linear chain with nonlinear resonator are different. Particularly, the former affects the waveform only in the short wavelength limit, while the latter can be tuned to affect the waveform in the long wavelength limit. These findings were also confirmed by the spectro-spatial analysis of such a nonlinear metamaterial presented in [34]. Note that both papers were limited to the study of the nonlinearity attributed to either the chain only or local resonator only. We did not examine the combination of both nonlinearities.

In this paper, we extend our work in [33,34] by combining both chain nonlinearity and local resonators nonlinearity and thoroughly study the relation between topological (i.e., space-time domain) and spectral (dispersion relations) features of a wave propagating in such a nonlinear metamaterial. We derive analytical expressions for the dispersion relations by the method of multiple scales. Our analytical results are validated through numerical simulation. Parametric studies are carried out to examine the role of both hardening and softening nonlinearities in the chain and local resonators. The results show very interesting characteristics of wave propagation in all wavelength limits.

The remainder of the paper is organized as follows. Section 2 presents the mathematical modeling of the proposed nonlinear metamaterial. We address the spectral analysis in Sect. 3 and the spectro-spatial analysis in Sect. 4. Section 5 summarizes the findings and provides suggestion for future work.

2 Mathematical modeling

This section presents the mathematical derivation for the dispersion equation for a nonlinear chain with nonlinear resonators depicted in Fig. 1. Each unit cell consists of a rigid mass, m, connected to other cells through a nonlinear spring with linear coefficient, k and nonlinear coefficient Γ. Inside each cell, there are multiple resonators with mass, m_i, attached by nonlinear spring with linear spring coefficient, k_i and nonlinear spring coefficient, Γ_i. The free oscillation equations for each cell with s number of resonators can be expressed as

$$\begin{aligned} m\ddot{u}_n &+ K(2u_n - u_{n-1} - u_{n+1}) \\ &+ \epsilon\Gamma((u_n - u_{n-1})^3 + (u_n - u_{n+1})^3) \\ &+ \sum_{i=1}^{s} k_i(u_n - v_{ni}) \\ &+ \sum_{i=1}^{s} \epsilon\Gamma_i(u_n - v_{ni})^3 = 0 \end{aligned} \tag{1}$$

$$m_i\ddot{v}_{ni} + k_i(v_{ni} - u_n) + \epsilon\Gamma_i(v_{ni} - u_n)^3 = 0 \tag{2}$$

For convenience, we introduce the following dimensionless parameters

$$\tau = \omega_n t;\ \bar{\Gamma} = \frac{\Gamma}{K};\ \bar{\Gamma_i} = \frac{\Gamma_i}{K};\ \bar{k_i} = \frac{k_i}{K} \tag{3}$$

where $\omega_n = \sqrt{K/m}$ and $\omega_{di} = \sqrt{k_i/m_i}$.

Introducing these parameters in Eqs. (1)–(2) leads to

$$\ddot{u}_n + 2u_n - u_{n-1} - u_{n+1} + \epsilon\bar{\Gamma}((u_n - u_{n-1})^3 + (u_n - u_{n+1})^3) + \sum_{i=1}^{s}\bar{k}_i(u_n - v_{ni}) + \sum_{i=1}^{s}\epsilon\bar{\Gamma}_i(u_n - v_{ni})^3 = 0 \tag{4}$$

$$\frac{\omega_n^2}{\omega_{di}^2}\ddot{v}_{ni} + (v_{ni} - u_n) + \epsilon\frac{\bar{\Gamma}_i}{\bar{k}_i}(v_{ni} - u_n)^3 = 0 \tag{5}$$

We assume expansions for the displacements in the form

$$u_n(t,\epsilon) = u_{n0}(T_0, T_1) + \epsilon u_{n1}(T_0, T_1) + o(\epsilon^2) \tag{6}$$

$$v_{ni}(t,\epsilon) = v_{ni0}(T_0, T_1) + \epsilon v_{ni1}(T_0, T_1) + o(\epsilon^2) \tag{7}$$

where $T_0 = \tau$ is the fast time scale and $T_1 = \epsilon\tau$ is the slow time scale. Since the time is expressed in two independent variables, the time derivative can be presented by using the chain role as

$$(\ddot{\ }) = D_0^2 + 2\epsilon D_0 D_1 + \ldots \tag{8}$$

where $D_n = \frac{\partial}{\partial T_n}$. Substituting Eqs. (6)–(8) into Eqs. (4)–(5) and collecting the similar coefficients of ϵ, one can get

Order ϵ^0

$$D_0^2 u_{n0} + 2u_{n0} - u_{(n-1)0} - u_{(n+1)0} + \sum_{i=1}^{s}\bar{k}_i(u_{n0} - v_{ni0}) = 0 \tag{9}$$

$$\frac{\omega_n^2}{\omega_{di}^2} D_0^2 v_{ni0} - (u_{n0} - v_{ni0}) = 0 \tag{10}$$

Order ϵ

$$D_0^2 u_{n1} + 2u_{n1} - u_{(n-1)1} - u_{(n+1)1} + \sum_{i=1}^{s}\bar{k}_i(u_{n1} - v_{ni1}) = -2D_0D_1u_{n0} - \bar{\Gamma}((u_{n0} - u_{(n-1)0})^3 + (u_{n0} - u_{(n+1)0})^3) - \sum_{i=1}^{s}\bar{\Gamma}_i(u_{n0} - v_{ni0})^3 \tag{11}$$

$$\frac{\omega_n^2}{\omega_{di}^2} D_0^2 v_{ni1} - (u_{n1} - v_{ni1}) = -2\frac{\omega_n^2}{\omega_{di}^2} D_0D_1v_{ni0} - \frac{\bar{\Gamma}_i}{\bar{k}_i}(v_{ni0} - u_{n0})^3 \tag{12}$$

2.1 Linear dispersion relation

At order ϵ^0, the problem is linear; therefore, the solution can be expressed as [22]

$$u_n = Ae^{j(nk-\omega T_0)} + c.c \tag{13}$$

$$v_{ni} = B_i e^{j(nk-\omega T_0)} + c.c \tag{14}$$

where $c.c$ refers to complex conjugate, $k = qa$ denotes the dimensionless wave number, and q represents the wave number. A and B_i stand for the wave amplitude of the outer and inner masses, respectively. By substituting Eqs. 13–14 into Eqs. 9–10 and following [22], the linear dispersion equation can be expressed as

$$-\omega^2 + (2 - 2\cos k) + \sum_{i=0}^{s}\bar{k}_i(1 - K_{\omega i}) = 0 \tag{15}$$

where $K_{\omega i} = \frac{\omega_{di}^2}{\omega_{di}^2 - \omega_n^2\omega^2}$.

2.2 Approximate analytical solution for the nonlinear dispersion relation

For small values of nonlinear spring coefficients, Γ and Γ_i, Eqs. (4)–(5) are classified as weakly nonlinear. For such a system, the nonlinear dispersion relations can be derived approximately by perturbation techniques. For system with multiple coupled equations, it is more convenient to employ the method of multiple scales since it has advantages over other methods in terms of the required efforts and associated algebra. By rearranging equations at order ϵ, we obtain

$$X(D_0^2u_{n1} + 2u_{n1} - u_{(n-1)1} - u_{(n+1)1}) + \sum_{i=1}^{s}\frac{X\bar{k}_i\omega_n^2/\omega_{di}^2}{1 - \omega_n^2\omega^2/\omega_{di}^2}D_0^2u_{n1} = \sum_{i=1}^{s}\frac{X\bar{k}_i}{1 - \omega_n^2\omega^2/\omega_{di}^2}(-2\omega_n^2/\omega_{di}^2 D_0D_1v_{ni0} + \frac{\bar{\Gamma}_i}{\bar{k}_i}(u_{n0} - v_{ni0})^3) + X(-2D_0D_1u_{n0} - \sum_{i=1}^{s}\bar{\Gamma}_i(u_{n0} - v_{ni0})^3 - \bar{\Gamma}((u_{n0} - u_{(n-1)0})^3 + (u_{n0} - u_{(n+1)0})^3)) \tag{16}$$

where $X = \prod_{i=1}^{s}(1 - \omega^2\omega_n^2/\omega_{di}^2)$.

Introducing Eqs. (13)–(14) into Eq. (16) leads to

$$X(D_0^2 u_{n1} + 2u_{n1} - u_{(n-1)1} - u_{(n+1)1}) + \sum_{i=1}^{s} \frac{X\bar{k}_i \omega_n^2/\omega_{di}^2}{1-\omega_n^2\omega^2/\omega_{di}^2} u_{n1} = \Bigg[2j\omega \sum_{i=1}^{s} \frac{X\bar{k}_i \omega_n^2/\omega_{di}^2}{1-\omega_n^2\omega^2/\omega_{di}^2} A' K_{\omega i} + 2jX\omega A' - 12\bar{\Gamma} X A^2 \bar{A}(1-\cos k)^2 + 3A^2\bar{A}\left(\sum_{i=1}^{s}\left[\frac{X(1-k_{\omega_i})^3}{1-\omega_n^2\omega^2/\omega_{di}^2}\bar{\Gamma}_i - X(1-k_{\omega_i})^3\bar{\Gamma}_i\right]\right)\Bigg] e^{j(nk-\omega T_0)} + NST \tag{17}$$

where NST denotes non-secular terms, $A' = \frac{\mathrm{d}A}{\mathrm{d}T_1}$, and $\bar{A}$ is the complex conjugate of A. We note here that X becomes $X = \prod_{i=1}^{s}(1-\omega^2\omega_n^2/\omega_{di}^2)$

The left-hand side of Eq. (17) has a nontrivial solution, while the secular terms on the right-hand side must be eliminated for bonded solution by solving the following solvability condition [19]

$$\Bigg[2j\omega \sum_{i=1}^{s} \frac{X\bar{k}_i \omega_n^2/\omega_{di}^2}{1-\omega_n^2\omega^2/\omega_{di}^2} A' K_{\omega i} + 2jX\omega A' - 12\bar{\Gamma} X A^2 \bar{A}(1-\cos k)^2 + 3A^2\bar{A}\left(\sum_{i=1}^{s}\left[\frac{X(1-k_{\omega_i})^3}{1-\omega_n^2\omega^2/\omega_{di}^2}\bar{\Gamma}_i - X(1-k_{\omega_i})^3\bar{\Gamma}_i\right]\right)\Bigg] = 0 \tag{18}$$

Substituting the polar form

$$A = \frac{1}{2}\alpha e^{j\beta} \tag{19}$$

into the solvability condition and separating the real and imaginary parts, the modulation equations for the amplitude and phase can be expressed as

$$\omega \sum_{i=1}^{s} \frac{\bar{k}_i X\omega_n^2/\omega_{di}^2}{1-\omega_n^2\omega^2/\omega_{di}^2}\alpha' K_{\omega i} + X\omega\alpha' = 0 \tag{20}$$

$$-\omega \sum_{i=1}^{s} \frac{\bar{k}_i X\omega_n^2/\omega_{di}^2}{1-\omega_n^2\omega^2/\omega_{di}^2}\alpha\beta' K_{\omega i} - X\omega\alpha\beta' - \frac{3}{2}X\bar{\Gamma}\alpha^3(1-\cos k)^2 - \sum_{i=1}^{s}\left[\frac{3}{8}\alpha^3(1-K_{\omega_i})^3 X\bar{\Gamma}_i \left(\frac{1}{1-\omega_n^2\omega^2/\omega_{di}^2} - 1\right)\right] = 0 \tag{21}$$

By solving the modulation equations, the amplitude and phase can be expressed as

$$\alpha = \alpha_0 \tag{22}$$

$$\beta = \frac{\sum_{i=1}^{s}\left[\frac{3}{8}\alpha^2(1-K_{\omega_i})^3\bar{\Gamma}_i\left(\frac{1}{1-\omega_n^2\omega^2/\omega_{di}^2} - 1\right)\right] - \frac{2}{3}\bar{\Gamma}\alpha^2(1-\cos k)^2}{\omega\left(1+\sum_{i=1}^{s}\frac{\bar{k}_i\omega_n^2/\omega_{di}^2}{1-\omega_n^2\omega^2/\omega_{di}^2}K_{\omega i}\right)} T_1 \tag{23}$$

Since $T_1 = \epsilon\tau$, the nonlinear frequency , ω_{nl} associated with k is

$$\omega_{nl} = \omega + \epsilon\beta' \tag{24}$$

The nonlinear dispersion relation presented by Eq. (24) includes the effect of both nonlinearity in the chain $\bar{\Gamma}$ and in the resonators $\bar{\Gamma}_i$). This expression is also valid for the cases of nonlinear chain only (i.e., $\Gamma_i = 0$) and nonlinear resonator only (i.e., $\Gamma = 0$). It can also be observed that only the effect of nonlinearity of the chain varies explicitly with the wave number. Moreover, the nonlinear correction coefficient $\epsilon\beta'$ is a function of vibration amplitude α, the nonlinear spring coefficient $\epsilon\Gamma$ (for the nonlinear chain), and $\epsilon\Gamma_i$ (for the nonlinear resonator). It is noteworthy that we assume the system is weakly nonlinear (i.e., $\epsilon << 1$), set $\alpha = 1$ in all subsequent sections, and vary the magnitude of nonlinear stiffness.

3 Predicting band structure boundaries by analytical dispersion relations

3.1 Validating the current model

To check the accuracy of the derived expression, we validate our results by using two different techniques. First, for the nonlinear chain with single linear resonator case, we compare our results with those obtained by Lindstedt–Poincare method in the literature. Second, we compare our results for the nonlinear resonator case and multiple resonators case by direct numerical integration. For the numerical integration, we simulate

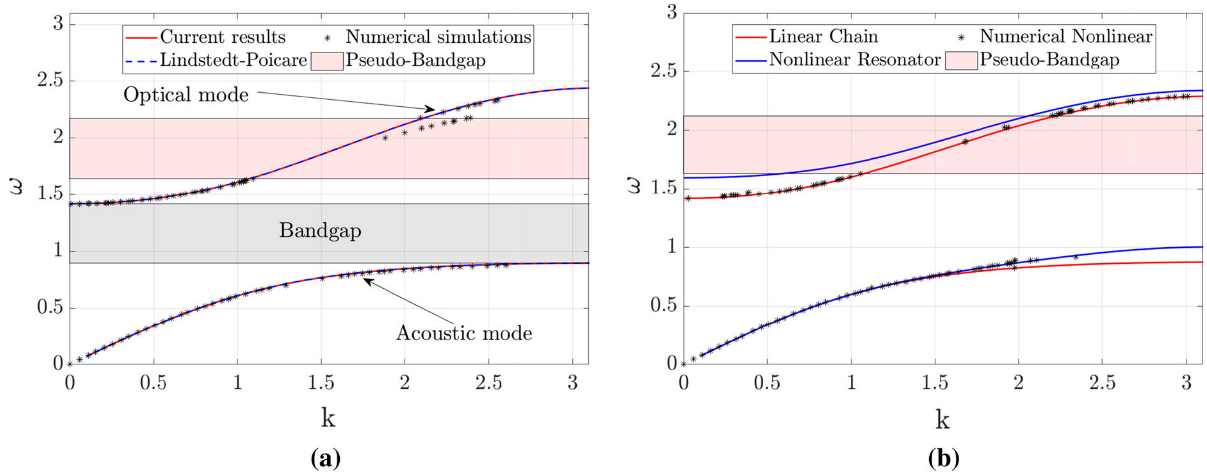

Fig. 2 **a** Validating the results of a nonlinear chain with single resonator $\alpha^2\epsilon\bar{\Gamma} = 0.06$, $\alpha^2\epsilon\bar{\Gamma}_1 = 0.$; **b** Validating the results of a linear chain with single nonlinear resonator $\alpha^2\epsilon\bar{\Gamma} = 0$, $\alpha^2\epsilon\bar{\Gamma}_1 = 0.06$

500 cells with perfectly match layers (PML) to omit wave reflections [21]. The system is excited by a transient wave packet applied at the beginning of the structure and propagating to the other end of the structure. The velocity of the wave packets is selected to force the wave to travel in one direction only and suppress any wave propagating in the opposite direction. This wave packet excitation can be defined as:

$$u_m(0) = \frac{1}{2}(H(m-1) - H(m-1-N_{cy}2\pi/k))$$
$$(1-\cos(mk/N_{cy}))\sin(mk) \quad (25)$$
$$\dot{u}_m(0) = \frac{1}{2}(H(m-1) - H(m-1-N_{cy}2\pi/k))$$
$$(-\omega_n\omega/N_{cy}\sin(mk/N_{cy})\sin(mk)$$
$$-\omega_n\omega(1-\cos(mk/N_{cy}))\cos(mk)) \quad (26)$$
$$v_{mi}(0) = K_{\omega i}u_m(0) \quad (27)$$
$$\dot{v}_{mi}(0) = K_{\omega i}\dot{u}_m(0) \quad (28)$$

where N_{cy} is the number of cycles and in our numerical simulations we set $N_{cy} = 7$, and $H(x)$ is the Heaviside function. For these initial conditions, we integrate the system by MATLAB built in integrator ODE45.

To obtain numerical dispersion curves, we collect the time response resulting from the numerical integration in the displacement matrix at a specific wave number. The displacement matrix is then transformed to the frequency–wave number domain by 2D fast Fourier transform (2D-FFT). We next pick the point with maximum power density. The frequency and wave number corresponding to this point are a point on the reconstructed dispersion curve. To construct the full curve, the wave number is swept along the first Brillouin zone.

The parameters of the system are selected as $\omega_n = \omega_{d1} = 1000$ rad/s, and $\bar{k}_1 = 1$ for single resonator system (i.e., s = 1), and for two resonators case (i.e., s=2) and we select the parameters as $\omega_n = \omega_{d1} = 1000$ rad/s, $\omega_{d2} = 1.5\omega_n$, $\bar{k}_1 = 1$, and $\bar{k}_2 = 1.5$.

Validation for the nonlinear chain and single linear resonator is presented in Fig. 2a. It is observed that our multiple-scale results show a good agreement with those obtained by the Lindstedt–Poincare method [32] and numerical results except inside the pseudo-bandgap. In the pseudo-bandgap region (as we will show in the subsequent sections), there is a significant frequency shift for wave packets excitation [32]. This significant frequency shift cannot be captured by our approximate solution. It is noteworthy here that we highlighted the bandgap, optical mode, and acoustic mode for single resonator system in Figs. 2 and 3.

For the cases of nonlinear resonators, the results are only validated numerically. The results of a chain with single nonlinear resonator are shown in Fig. 2b. The numerical results show a good agreement with the analytical results in the acoustic mode. However, a significant error is observed near the resonator frequency. This error results from the significant frequency shift. Indeed, points in the long wavelength limit ($k \sim 0$ since $\lambda = 2\pi/k$ where λ is the wavelength) belong to a signal with wavelength inside the pseudo-bandgap (at medium wavelength limit $k \sim \pi/2$); however, due to

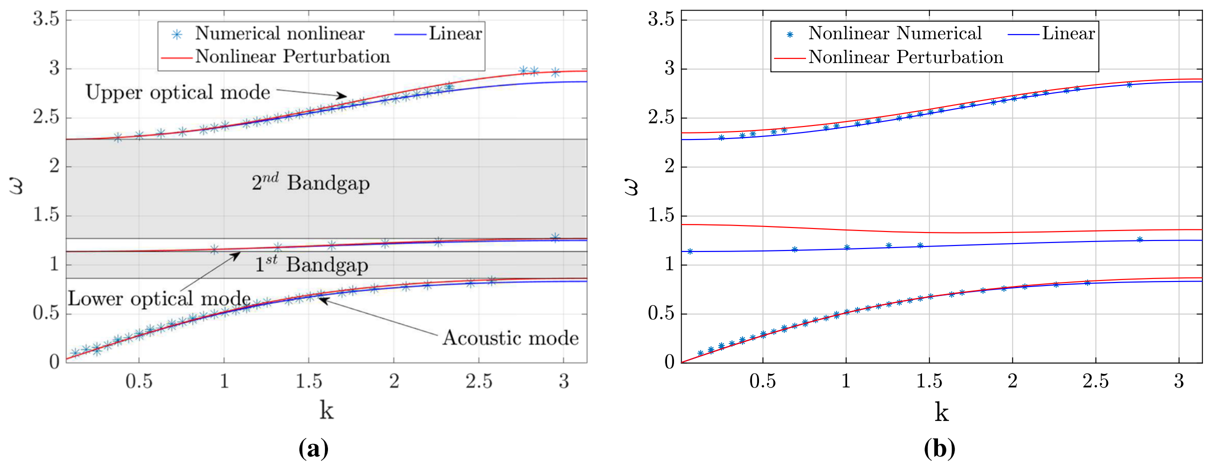

Fig. 3 **a** Validating the results of a nonlinear chain with multiple resonator $\alpha^2\epsilon\bar{\Gamma} = 0.06$, $\alpha^2\epsilon\bar{\Gamma}_1 = \alpha^2\epsilon\bar{\Gamma}_2 = 0.$; **b** Validating the results of a linear chain with multiple nonlinear resonator $\alpha^2\epsilon\bar{\Gamma} = \alpha^2\epsilon\bar{\Gamma}_2 = 0$, $\alpha^2\epsilon\bar{\Gamma}_1 = 0.06$

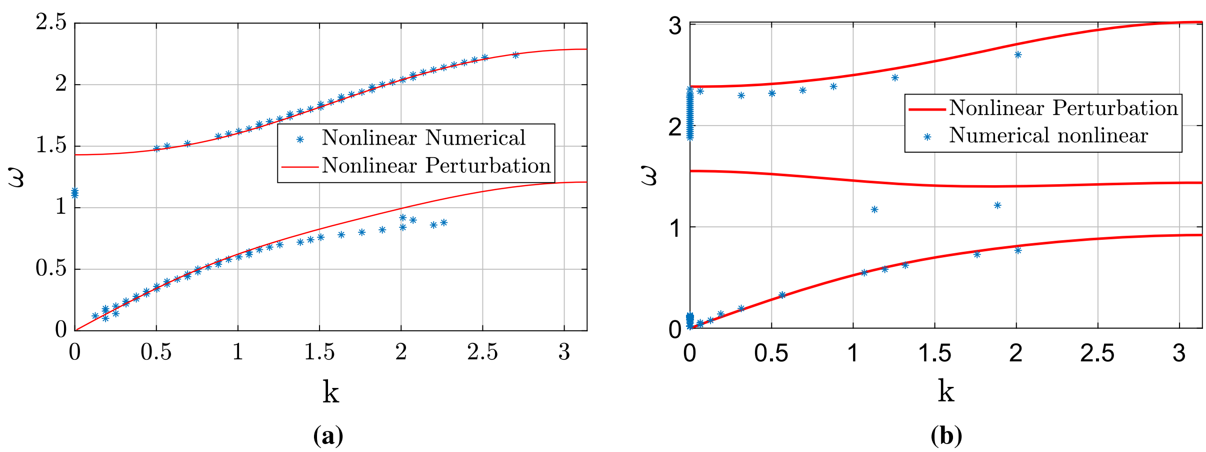

Fig. 4 **a** Validating the results of a nonlinear chain with single nonlinear resonator $\alpha^2\epsilon\bar{\Gamma} = \alpha^2\epsilon\bar{\Gamma}_1 = 0.06.$; **b** Validating the results of a linear chain with multiple nonlinear resonators $\alpha^2\epsilon\bar{\Gamma} = \alpha^2\epsilon\bar{\Gamma}_1 = \alpha^2\epsilon\bar{\Gamma}_2 = 0.06$

the significant frequency shift, they appear in the long wavelength limit.

For multiple resonators, the results for nonlinear chain and nonlinear resonators are presented in Fig. 3. We note here that reconstructing the dispersion curves by wave packets excitation is not possible due to the significant frequency shift. Therefore, we reconstruct the dispersion curves using a plane waves excitation. For a nonlinear metamaterial with linear local resonators (i.e., Fig. 3a), the perturbation results can accurately predict the cutoff frequencies. On the other hand, in the case of linear chain with nonlinear resonators, the perturbation results can only predict cutoff frequencies away from the surrounding region of nonlinear resonator frequency. Hence, higher-order perturbations or other nonlinear analytical tools may be required to provide better approximations.

Validation of results for a metamaterial with combined nonlinearity in both cells and resonators is presented in Fig. 4. The results show very good agreement between our analytical and numerical methods. However, similar observation can be revealed about the failure in predicting the dispersion curves near the frequency of nonlinear resonator. This is clearly demonstrated in Fig. 4a in the short wavelength ($k \sim \pi$) limit of the acoustic branch and long wavelength limit of the optical branch. The points in these regions cannot be captured numerically. For multiple resonators case (Fig. 4b), a significant frequency shift is observed in the middle branch. This region of frequency shift is confined between the frequencies of both nonlinear resonators.

3.2 Analytical band structure for different sources and types of nonlinearities

The numerical validation in Sect. 3.1 revealed that the analytical dispersion curves can predict the regions of wavelength that are affected by nonlinearity although they fail in accurately estimating the band structure limits. In addition to Figs. 2, 3, and 4, dispersion curves for different sources and types of nonlinearities are depicted in Figs. 5 and 6.

For single resonator system, the effect of softening nonlinearity on the band structure is depicted in Fig. 5a. It is observed that the dispersion curves shift due to nonlinear resonator is more pronounced at frequencies close to the bandgap. This means that the short wavelength region in the acoustical mode and the long wavelength region in the optical mode are significantly affected by the nonlinear resonator. On the other hand, the dispersion curves shift for the nonlinear chain is confined in the short wavelength regions in both modes. This is not surprising since the nonlinear correction term β' explicitly depends on the wave number for the case of nonlinear chain unlike the case of nonlinear resonator. It is noteworthy that softening chain increases the size of the bandgap; however, the softening resonator does not.

The dispersion curves for a system with nonlinear chain and nonlinear local resonators with the same type of nonlinearity are plotted in Fig. 5b. When the type of nonlinearity is hardening, the dispersion curves are significantly shifted up. However, the dispersion curves are shifted down for softening type of nonlinearity. This shift is concentrated in the short wavelength region in the acoustic mode. The resonators nonlinearities equally shift the optical mode in all wavelength regions. This shift in the optical mode in the short wavelength limit can be attributed to the chain nonlinearity, whereas that in the long wavelength limit is due to resonator nonlinearity.

To clarify the affected wavelength regions, we assign different types of nonlinearities for the chain and local resonators as depicted in Fig. 5c. It is demonstrated that the local resonator nonlinearity is more dominant than chain nonlinearity in the acoustic mode. However, there are different effects on the dispersion curves shifts in the optical mode. This difference is demonstrated by domination of the local resonance nonlinearity in the long wavelength region and domination of the chain nonlinearity in the short wavelength region. Furthermore, there is an interaction between both sources of nonlinearities in medium wavelength ($k \sim \pi/2$) region since the nonlinear curves intersect the linear curve in Fig. 5c.

For the multiple resonators case, the effect of each source and type of nonlinearity on the dispersion curves is shown in Fig. 5d–f. The shift attributable to nonlinear chain is pronounced in the short wavelength regions similar to the single resonator case as shown in Fig. 5d. However, the impact of nonlinear resonators on the dispersion curves is not concentrated at the bandgap boundaries. Instead, it is related to the tuned frequency of the nonlinear resonator. For instance, if the resonator with $\omega_{d1} = \omega$ is nonlinear, we observe a substantial dispersion curves shift near $\omega = 1$ as shown in Fig. 5e. Similarly, the dispersion curves shift is observed at frequencies close to $\omega = 1.5$ when the nonlinear resonator is the second resonator $\omega_{d2} = 1.5\omega$ as shown in Fig. 5f.

To further illustrate the effect of nonlinearity on dispersion curves for the case of multiple local resonators, we investigate the nonlinear system when the chain and all local resonators are both nonlinear. The results are depicted in Fig. 6. When the chain and local resonators have all the same type of nonlinearity (softening or hardening), the dispersion curves are shifted up in all modes as demonstrated in Fig. 6a. This shift is quantitatively variant; however, its trend is not.

Next, we assign different types of nonlinearity to the chain and local resonators. The results are shown in Fig. 6b and reveal that the impact of nonlinearity in the chain can be observed only in the second optical mode at the short wavelength limit. This is not surprising since that zone is away from the local resonators frequencies; therefore, the effect of nonlinear local resonators is not dominant there.

Finally, the effect of each nonlinear local resonators on wavelength zones can be obtained from Fig. 6c, d. The figures show that when one of the nonlinear local resonators has a nonlinearity type different than the nonlinearity of the chain and the other local resonator, the impact of that resonator is dominant in the short

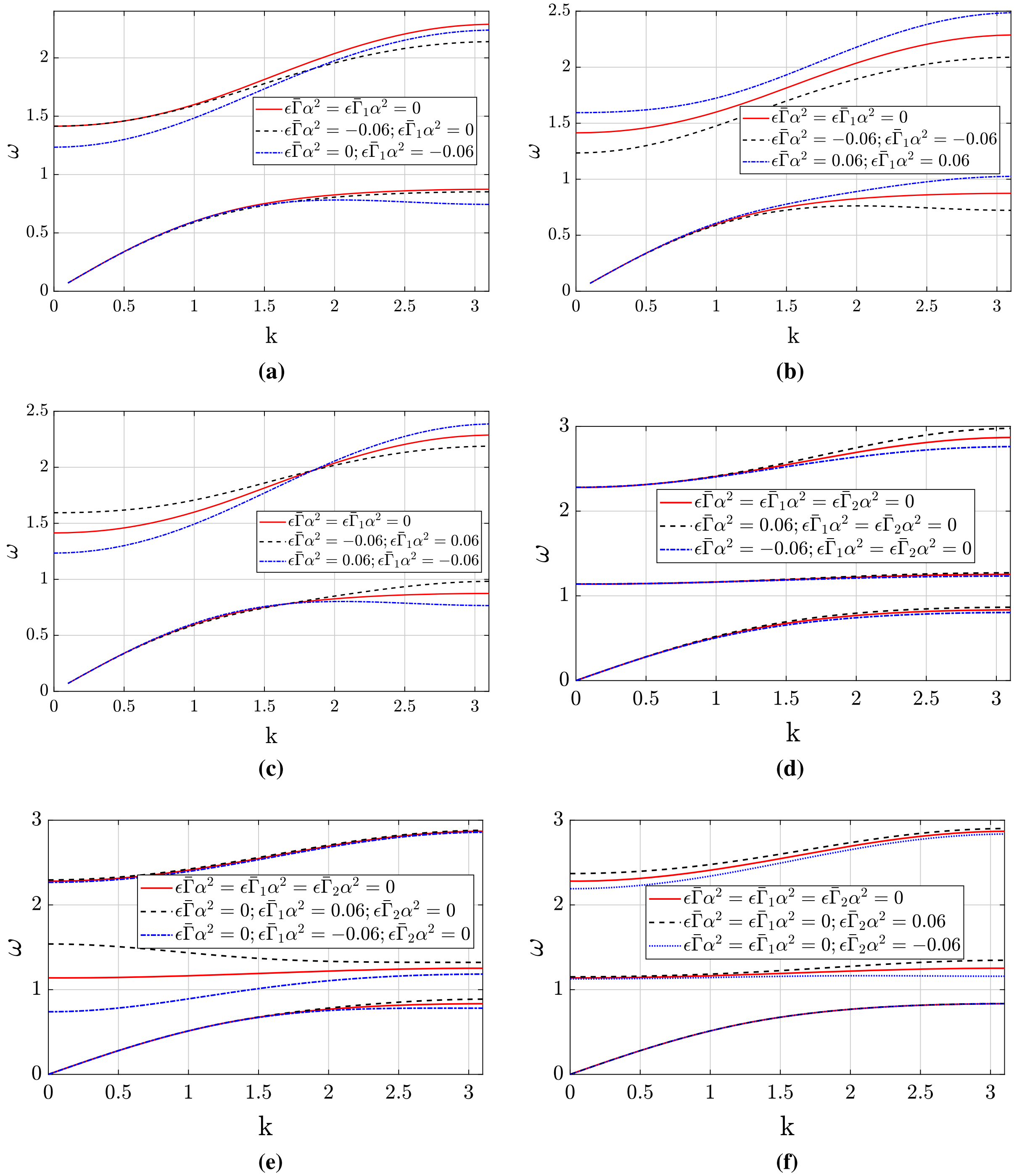

Fig. 5 Analytical band structure for a system with single and multiple resonators and different sources and types of nonlinearities. **a**–**c**: single resonator and **d**–**f** two resonators

wavelength limit in the mode just below its frequency and in the long wavelength limit in the upper branch. The results here suggest that for the case of multiple resonators, the dispersion curves shift due to nonlinear local resonator is dominant in frequency zones near its tuned frequency. Therefore, tuning the nonlinear res-

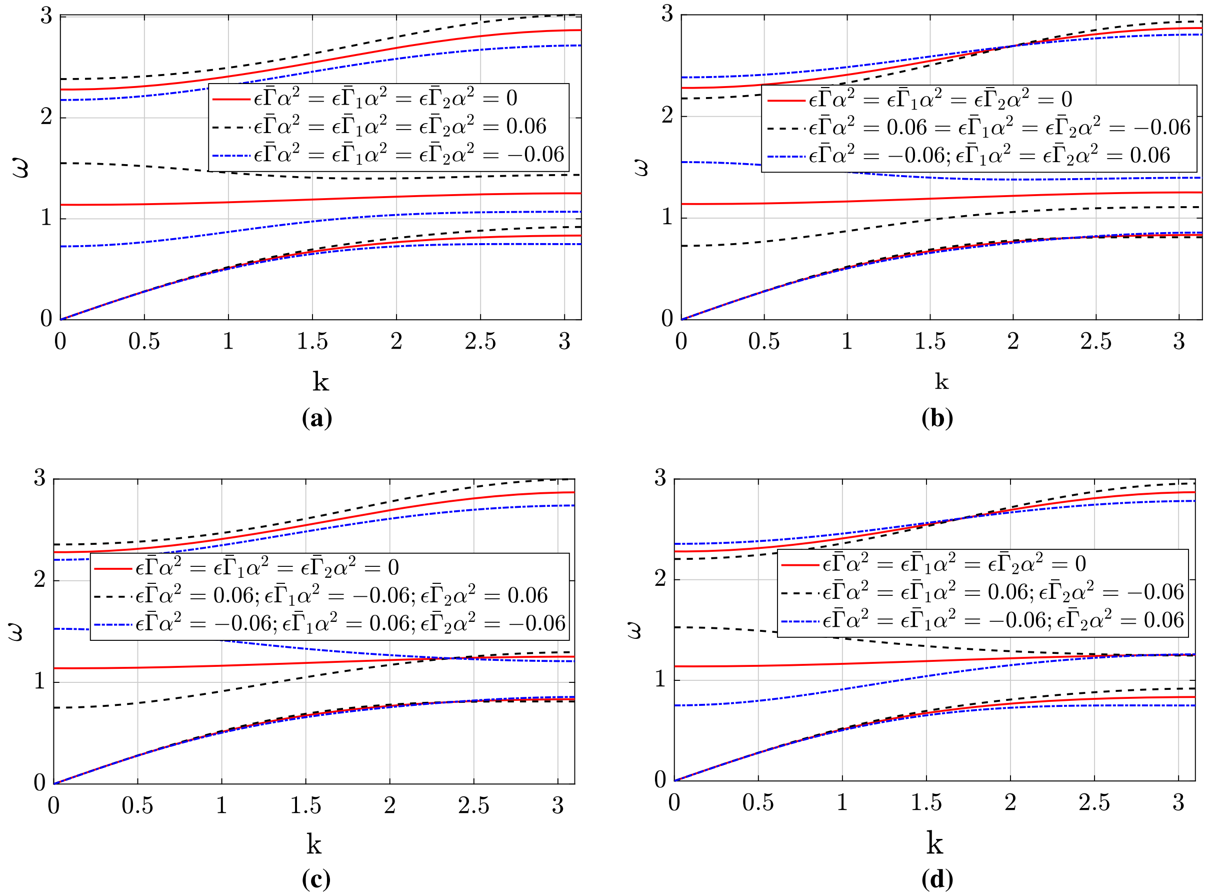

Fig. 6 Analytical band structure for a system with single and multiple resonators and different sources and types of nonlinearities

onator is crucial in determining the zones affected by nonlinearity. Solitary waves, wave non-reciprocity, and other nonlinear phenomena can be observed in these zones. On the other hand, zones at short wavelength limit and away from the resonator frequency are only affected by nonlinear chain.

4 Spectro-spatial analysis

Although the cutoff frequencies (boundaries of the nonlinear band structures) can be predicted by the method of multiple scales, other nonlinear wave propagation features (e.g., solitons, secondary resonances, dispersive waves) cannot be characterized. This suggests the use of spectro-spatial analysis to characterize the wave propagation in the proposed metamaterial. It should be noted that all the following simulations are based on the optical (upper branch) wave mode because we find this mode to be more affected by nonlinearity than the acoustic mode. In particular, there is no significant frequency shift observed in the acoustics branch (also defined as pseudo-bandgap in Sect. 3.1) and it is hard to tune the nonlinear resonator to the long wavelength region in this mode. Otherwise, the observation in the optical mode should be similar to those in the acoustic mode. Also the numerical simulation for the optical mode is much faster. The simulation in this mode lasted for 8 s, while the wave packet defined in Eqs. (25)–(28) was used as an input signal.

4.1 Spatial profile of the wave packet

At the end of the simulation, the spatial profiles of the wave packet are plotted in Figs. 7 and 8. To investigate how each source of nonlinearity alters the input signal, we first present the wave profile of a metamaterial with

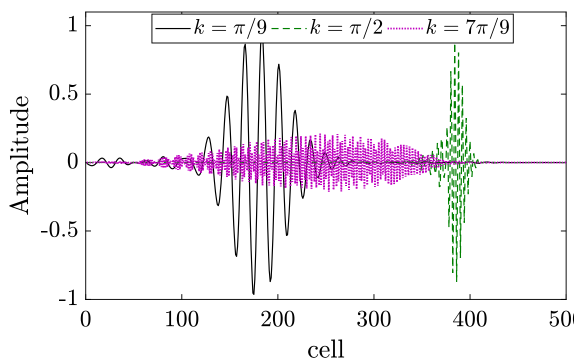

(a) Linear chain: $\epsilon\bar{\Gamma}\alpha^2 = \epsilon\bar{\Gamma}_1\alpha^2 = \epsilon\bar{\Gamma}_2\alpha^2 = 0$

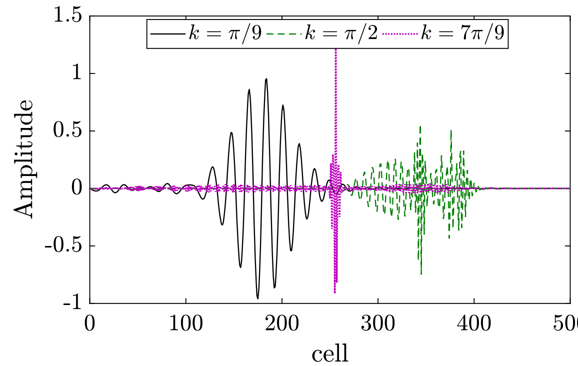

(b) Hardening chain nonlinearity $\epsilon\bar{\Gamma}\alpha^2 = 0.03$, $\epsilon\bar{\Gamma}_1\alpha^2 = \epsilon\bar{\Gamma}_2\alpha^2 = 0$

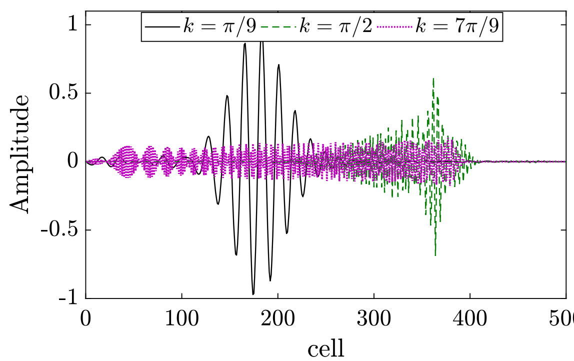

(c) Softening chain nonlinearity $\epsilon\bar{\Gamma}\alpha^2 = -0.03$, $\epsilon\bar{\Gamma}_1\alpha^2 = \epsilon\bar{\Gamma}_2\alpha^2 = 0$

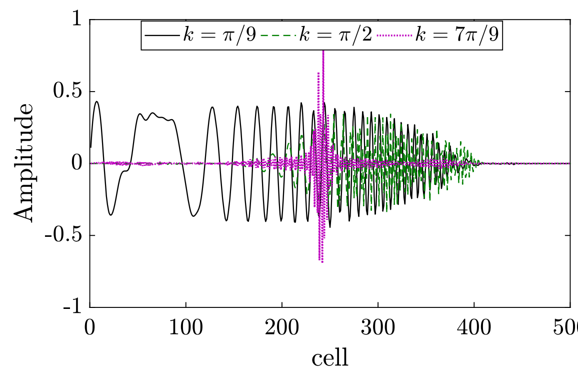

(d) Hardening resonator nonlinearity $\epsilon\bar{\Gamma}_2\alpha^2 = 0.03$, $\epsilon\bar{\Gamma}_1\alpha^2 = \epsilon\bar{\Gamma}\alpha^2 = 0$

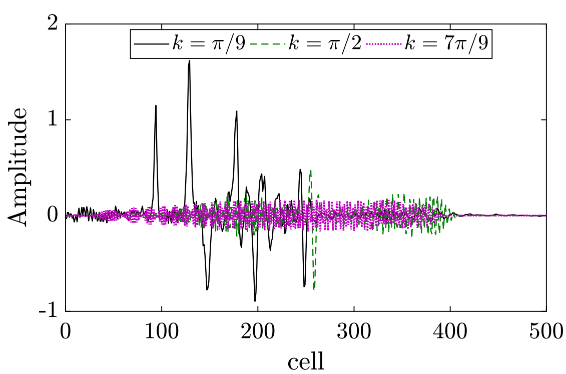

(e) Softening resonator nonlinearity $\epsilon\bar{\Gamma}_2\alpha^2 = -0.03$, $\epsilon\bar{\Gamma}_1\alpha^2 = \epsilon\bar{\Gamma}\alpha^2 = 0$

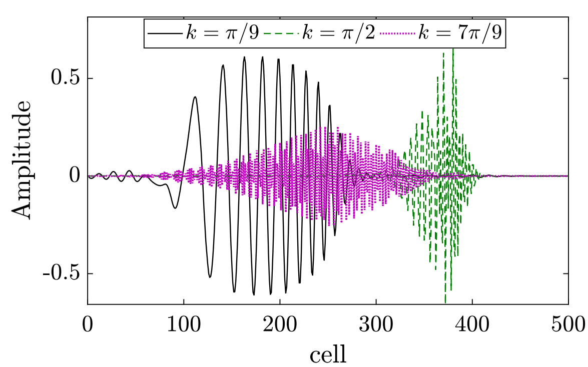

(f) Hardening resonator nonlinearity $\epsilon\bar{\Gamma}_1\alpha^2 = 0.03$, $\epsilon\bar{\Gamma}_2\alpha^2 = \epsilon\bar{\Gamma}\alpha^2 = 0$

Fig. 7 Spatial profile of the wave packet for different types and sources of nonlinearities at frequencies in the upper branch of dispersion curve

a single source of nonlinearity in Fig. 7. The wave profile for a signal propagating in a linear chain is shown in Fig. 7a. The results show that the wave is not distorted in the long wavelength limit. However, the wave becomes gradually dispersive with the increase in wave number (i.e., the amplitude of the wave becomes lower at high wave number since waves of different frequencies travel with different phase speeds. We refer the reader to Figure 9 in [25] for more information).

It should be noted that the terms distortion and dispersive are not exactly the same although they both indicate deformation in the input wave. We used the former mainly when the wave is split into multiple components and/or when there are other forms of deformation resulting from nonlinearity in the system. The latter is used when the wave get stretched and the wave amplitude becomes smaller.

For nonlinear chain only, there is no effect on the wave profile in the long wavelength range and the nonlinear chain behaves like the linear chain as shown in Fig. 7b, c. This is not surprising since inspecting Eq. (23) when $\bar{\Gamma}_i = 0$ demonstrates that for small values of wave numbers, β is negligible. In the meantime, increasing the wave number gradually shows different types of wave distortion due to nonlinear chain. For instance, hardening chain distorts the wave into a low-amplitude dispersive signal and high-amplitude localized signal. The latter indicates the birth of solitary wave due to nonlinearity unlike the pure dispersive signal in the linear case. This can be explained by changing the shape of the variable slope dispersion curve to linear (fixed slope) dispersion curve similar to those of nondispersive mediums in homogeneous structures [25] (see Sect. 4.3). On the other hand, softening chain stretches the signal further to lower-amplitude components with the absence of any localized high-amplitude signals. In other words, the shape of the variable slope dispersion curve of linear metamaterial becomes more nonlinear (variable slope), thus more dispersive [25].

The effect of some nonlinear phenomena in the long wavelength limit can be observed only when the nonlinearity is assigned in the resonator as depicted in Fig. 7d–f. If the resonator with a frequency near the upper dispersion curve is nonlinear, a significant distortion in the wave profile is observed in the vicinal frequencies. Therefore, nonlinearity in the local resonator can affect the long wavelength limit unlike the nonlinear chain case. For instance, we set the second resonator ($\omega_{d2} = 1.5\omega$) to be nonlinear and plot the wave profile in Fig. 7d, e. The results indicate that both hardening nonlinearity and softening nonlinearity in the resonator distort the wave shape at all wavelength limits. However, this distortion (w.r.t linear case in Fig. 7a) becomes less significant with the increase in wave number. The hardening nonlinearity stretches the wave in the long wavelength limit while it develops a localized signal in addition to the dispersive signal with the decrease in wavelength as shown in Fig. 7d. The softening nonlinearity stretches the wave profile more substantially at all wavelengths limits as shown in Fig. 7e. This dispersive signal is associated with multiple high-amplitude localized features with the increase in wavelength. Finally, we set the first resonator ($\omega_{d1} = \omega$) to be nonlinear and plot the wave profile in Fig. 7f. Since this resonator's frequency is away from the upper branch of dispersion curve, the effect of nonlinearity is insignificant. Figure 7f also shows the existence of a minor distortion in the wave profile at the long wavelength limit. This distortion becomes negligible with the increase in wave number.

After analyzing each type of nonlinearity individually, we analyze the effect of different combinations of nonlinearities as depicted in Fig. 8. When the chain and both resonators have hardening nonlinearity, waves at short wavelength limit form a solitary wave (localized signal) with a small-amplitude dispersive signal as shown in Fig. 8a. However, distortion at long wavelength limit is not negligible anymore since the nonlinear resonators stretch the wave with medium vibration amplitude. Between the long and short wavelength limits, there is a transition in the wave profile behavior, such that the wave has a dispersive feature (with amplitude in between the two limits) and localized feature with medium amplitude. Severe distortions in the wave profile are observed when the nonlinearity of both resonators is changed to softening as shown in Fig. 8b. Signals at all wavelength limits are more dispersive, particularly, waves with low wave numbers. However, one can still recognize localized features at short wavelength limit due to hardening chain. The latter can completely disappear if the chain has softening nonlinearity (see Fig. 8c), even though both resonators have hardening nonlinearity. Yet hardening nonlinear resonators reduce the wave stretching.

Next, we assign for the first resonator, a type of nonlinearity different from the second resonator, which has a frequency near the upper optical mode in Fig. 8d, e. It is observed that the behavior of the wave profile for the cases in Fig. 8d is similar to the wave profile in Fig. 8b and signals in Fig. 8e, a are also similar. Though the distortion in the mid- and long wavelength limits is less dominant by the nonlinearity of the second resonator, one can hypothesize that the effect of nonlinearity in the first resonator is less pronounced than that of the second resonator in the upper branch of the dispersion

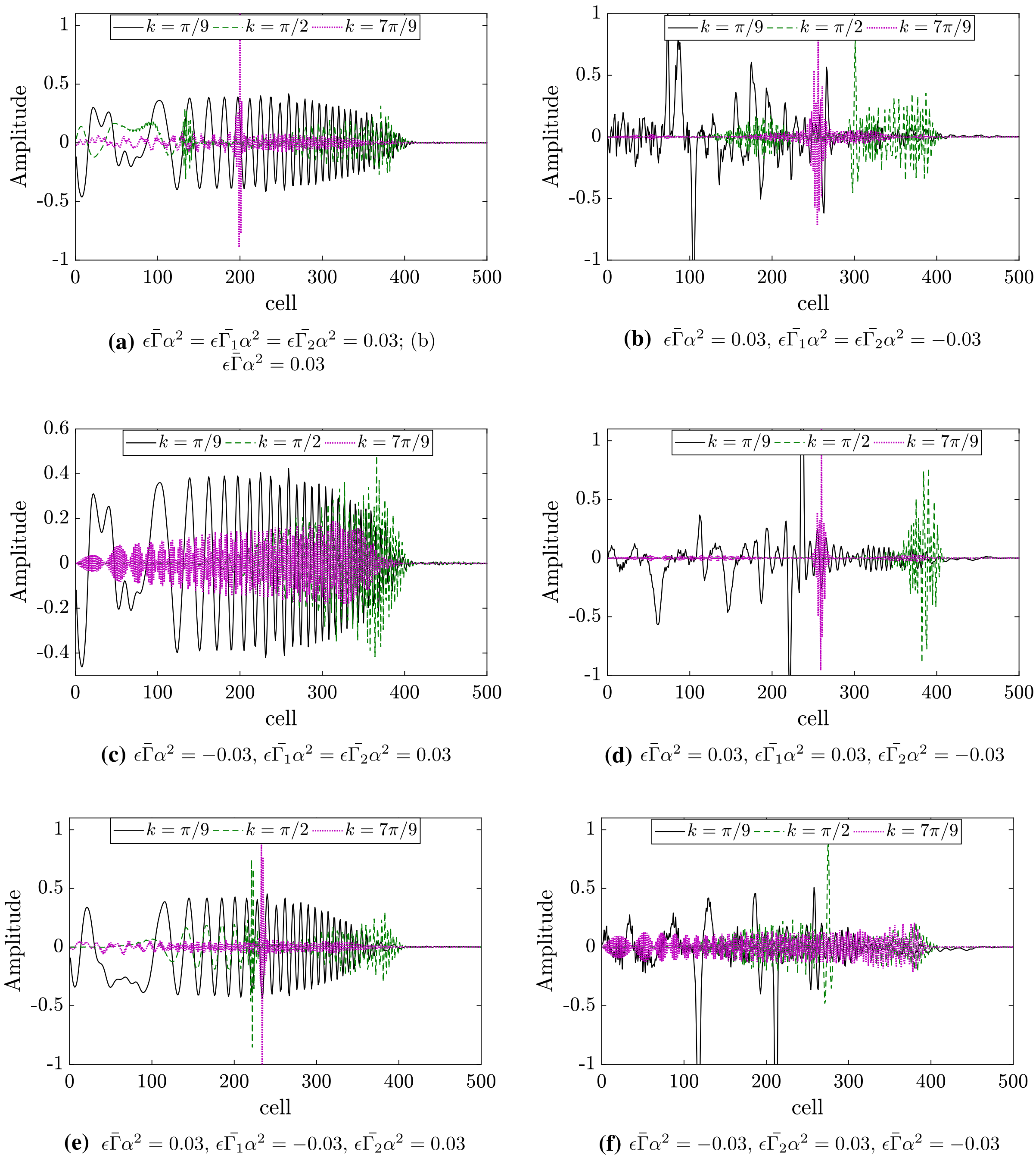

(a) $\epsilon\bar{\Gamma}\alpha^2 = \epsilon\bar{\Gamma}_1\alpha^2 = \epsilon\bar{\Gamma}_2\alpha^2 = 0.03$; (b) $\epsilon\bar{\Gamma}\alpha^2 = 0.03$

(b) $\epsilon\bar{\Gamma}\alpha^2 = 0.03$, $\epsilon\bar{\Gamma}_1\alpha^2 = \epsilon\bar{\Gamma}_2\alpha^2 = -0.03$

(c) $\epsilon\bar{\Gamma}\alpha^2 = -0.03$, $\epsilon\bar{\Gamma}_1\alpha^2 = \epsilon\bar{\Gamma}_2\alpha^2 = 0.03$

(d) $\epsilon\bar{\Gamma}\alpha^2 = 0.03$, $\epsilon\bar{\Gamma}_1\alpha^2 = 0.03$, $\epsilon\bar{\Gamma}_2\alpha^2 = -0.03$

(e) $\epsilon\bar{\Gamma}\alpha^2 = 0.03$, $\epsilon\bar{\Gamma}_1\alpha^2 = -0.03$, $\epsilon\bar{\Gamma}_2\alpha^2 = 0.03$

(f) $\epsilon\bar{\Gamma}\alpha^2 = -0.03$, $\epsilon\bar{\Gamma}_2\alpha^2 = 0.03$, $\epsilon\bar{\Gamma}\alpha^2 = -0.03$

Fig. 8 Spatial profile of the wave packet for different types and sources of nonlinearities at frequencies in the upper branch of dispersion curve

curves. Finally, we can also observe that the nonlinearity type in the first resonator does not distort the wave profile in the short wavelength limit since the frequency of this resonator is away from frequencies of the system in this region and the effect of other sources of nonlinearity are more dominant as shown in Fig. 8.

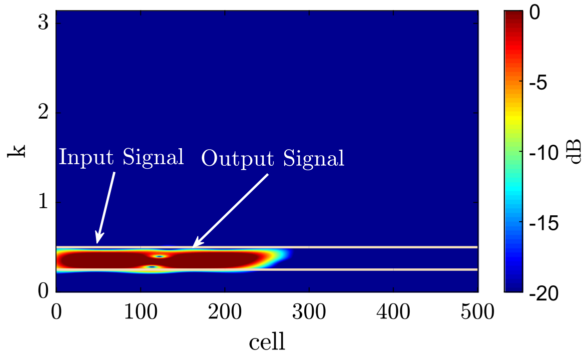

(a) Hardening chain nonlinearity $\epsilon\bar{\Gamma}\alpha^2 = 0.03$, $\epsilon\bar{\Gamma}_1\alpha^2 = \epsilon\bar{\Gamma}_2\alpha^2 = 0$, $k = \pi/9$

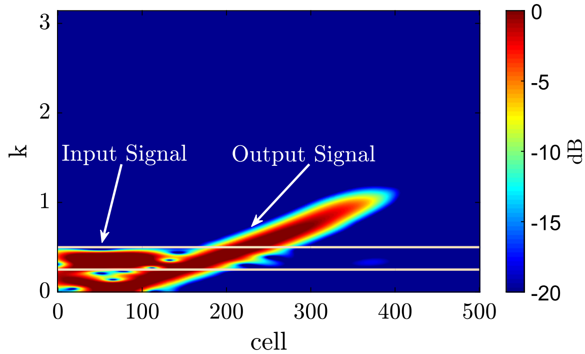

(b) Hardening resonator nonlinearity $\epsilon\bar{\Gamma}_2\alpha^2 = 0.03$, $\epsilon\bar{\Gamma}_1\alpha^2 = \epsilon\bar{\Gamma}\alpha^2 = 0$, $k = \pi/9$

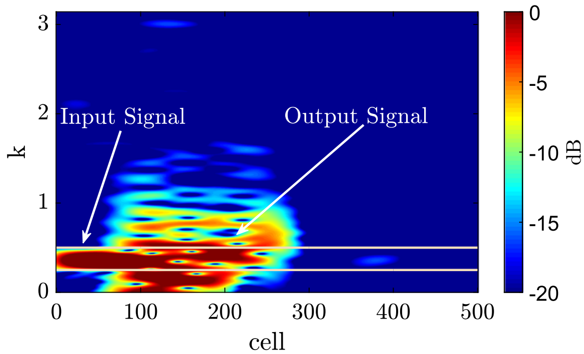

(c) Softening resonator nonlinearity $\epsilon\bar{\Gamma}_2\alpha^2 = -0.03$, $\epsilon\bar{\Gamma}_1\alpha^2 = \epsilon\bar{\Gamma}\alpha^2 = 0$, $k = \pi/9$

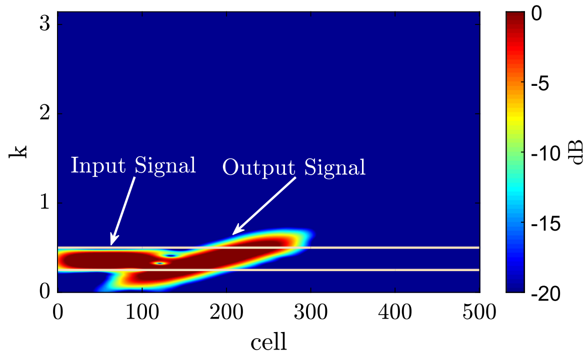

(d) Hardening resonator nonlinearity $\epsilon\bar{\Gamma}_1\alpha^2 = 0.03$, $\epsilon\bar{\Gamma}_2\alpha^2 = \epsilon\bar{\Gamma}\alpha^2 = 0$, $k = \pi/9$

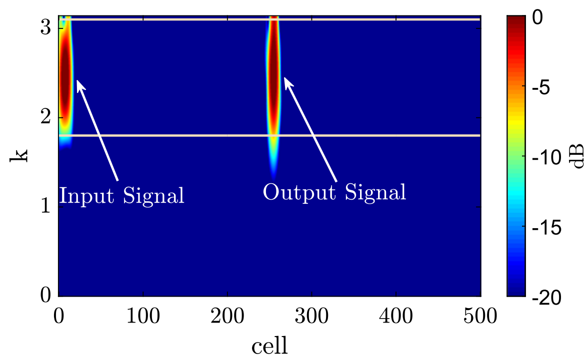

(e) Hardening resonator nonlinearity $\epsilon\bar{\Gamma}_2\alpha^2 = 0.03$, $\epsilon\bar{\Gamma}_1\alpha^2 = \epsilon\bar{\Gamma}\alpha^2 = 0$, $k = 7\pi/9$

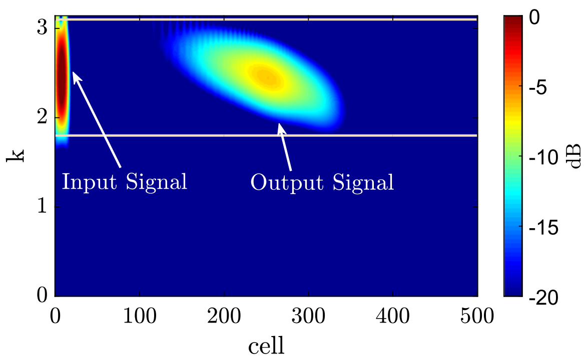

(f) Hardening resonator nonlinearity $\epsilon\bar{\Gamma}_1\alpha^2 = 0.03$, $\epsilon\bar{\Gamma}_2\alpha^2 = \epsilon\bar{\Gamma}\alpha^2 = 0$, $k = 7\pi/9$

Fig. 9 Spatial spectrograms of the wave packet for different types and sources of nonlinearities at frequencies in the upper branch of dispersion curve

4.2 Spatial spectrograms of the wave packet

After investigating wave propagation through the metamaterial in the spatial domain, we now examine the wave profile in the wave number domain. Here, we use short-term Fourier transform (STFT) instead of simple Fourier transform (FT) to investigate the signal as it changes over time. We apply a Hann window with the size of initial wave profile to divide the time signal into shorter segments. The spectrograms for different types

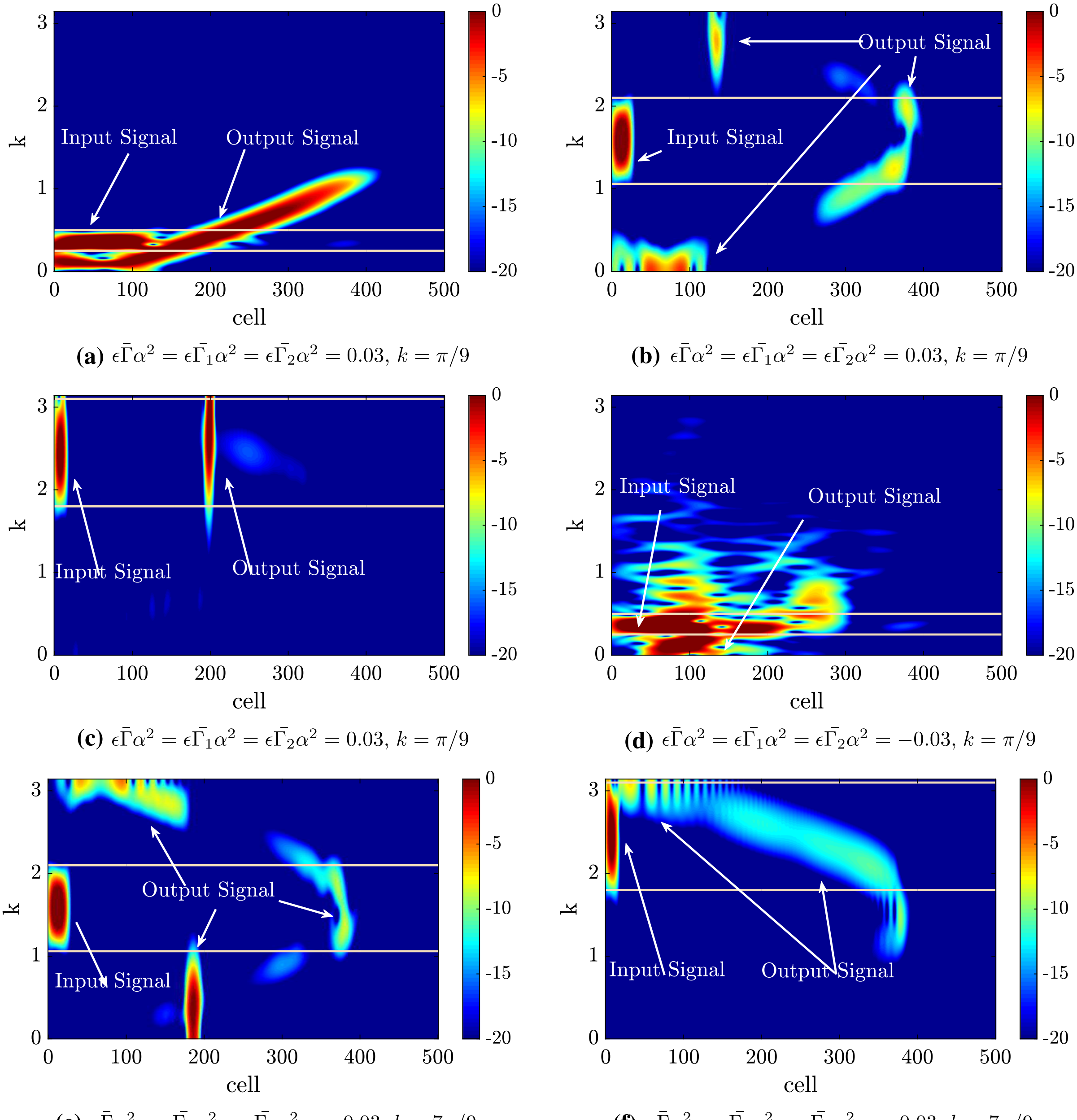

(a) $\epsilon\bar{\Gamma}\alpha^2 = \epsilon\bar{\Gamma_1}\alpha^2 = \epsilon\bar{\Gamma_2}\alpha^2 = 0.03,\ k = \pi/9$

(b) $\epsilon\bar{\Gamma}\alpha^2 = \epsilon\bar{\Gamma_1}\alpha^2 = \epsilon\bar{\Gamma_2}\alpha^2 = 0.03,\ k = \pi/9$

(c) $\epsilon\bar{\Gamma}\alpha^2 = \epsilon\bar{\Gamma_1}\alpha^2 = \epsilon\bar{\Gamma_2}\alpha^2 = 0.03,\ k = \pi/9$

(d) $\epsilon\bar{\Gamma}\alpha^2 = \epsilon\bar{\Gamma_1}\alpha^2 = \epsilon\bar{\Gamma_2}\alpha^2 = -0.03,\ k = \pi/9$

(e) $\epsilon\bar{\Gamma}\alpha^2 = \epsilon\bar{\Gamma_1}\alpha^2 = \epsilon\bar{\Gamma_2}\alpha^2 = -0.03,\ k = 7\pi/9$

(f) $\epsilon\bar{\Gamma}\alpha^2 = \epsilon\bar{\Gamma_1}\alpha^2 = \epsilon\bar{\Gamma_2}\alpha^2 = -0.03,\ k = 7\pi/9$

Fig. 10 Spatial spectrograms of the wave packet for different types and sources of nonlinearities at frequencies in the upper branch of dispersion curve

and sources of nonlinearities at different wavelengths are plotted in Figs. 9 and 10.

Figure 9a shows that the input signal is the same as the output signal for the case of nonlinear chain. This is not surprising since it was observed in the previous analysis that at long wavelength limit, the system with nonlinear chain has similar performance to the linear system. This does not hold in the nonlinear resonator case. It is revealed for Fig. 9b, c that the input signal is severely distorted in the long wavelength limit. If the nonlinearity is hardening, the input signal becomes stretched over the chain with high amplitude as shown in Fig. 9b. On the other hand, softening nonlinearity distorts the input signal into low-amplitude dispersive component and multiple high-amplitude localized components. Indeed, some of the energy content of the input signal appears at wave numbers outside the input signal window. This implies that this energy content appears at frequencies different than the input signal frequencies since wave number and frequency are related in Eq. (24). Therefore, we will refer to any shift in the wave number of the output signal as frequency shift in the subsequent discussion. However, if only the first resonator is nonlinear, the observed distortion is less significant at long wavelength limit as shown in Fig. 9d. Beyond the long wave length limit, the effect of nonlinearity in the case of nonlinear resonator is also demonstrated in the short wavelength limit as shown in Fig. 9e. We can observe that the nonlinear hardening resonator acts like the nonlinear hardening chain in the short wavelength limit, such that it distorts the signal into localized component unlike the dispersive signal in the linear chain. Since the short wavelength limit frequencies in the upper optical mode are away from the first resonator frequency, the effect of nonlinearity in this resonator is insignificant in this zone. For instance, we assign a hardening nonlinearity for this resonator in Fig. 9f, yet the wave is dispersive like the linear case.

To investigate how different types and sources of nonlinearities interact in the metamaterial, we assign different types of nonlinearity to the chain and resonators and plot them in Fig. 10. When all sources of nonlinearity are of hardening type, the system performs like the hardening resonator (ω_{d2}) in the long wavelength limit as depicted in Fig. 10a. Therefore, this zone can be controlled fully by the second resonator regardless of the nonlinearity in the chain, and partially by the first resonator as observed in Fig. 9d. In Fig. 10b, the output signal is distorted severely and brakes down into multiple components. Most of the energy content of the output signal appear at wave numbers away from the input signal wave numbers. Therefore, a significant frequency shift is observed at medium wavelength limit when all sources of nonlinearities are hardening. This frequency shift forms a pseudo-bandgap [32], which can be utilized to design acoustic diode. However, there is no frequency shift at short wavelength limit for hardening chain and hardening resonators, instead the signal is concentrated in a main component forming a solitary wave as depicted in Fig. 10c.

In order to generate a significant frequency shift in all wavelengths limits, we assign softening nonlinearity to both the resonators and the chain. This can generate a significant frequency shift in wavelength zones; therefore, it can widen the pseudo-bandgap, thus resulting in a wider operating frequency range for acoustic diodes for example. These plots are presented in Fig. 10d, e. A significant frequency shift is observed in all of these figures. In particular, the signal at long and medium wavelengths shifts the dominant component in the signal to very low values of wave number/frequency. This indicates that a wider pseudo-bandgap can be established at these wavelength zones, since any input signal with wave number/frequency in this range will be distorted and shifted significantly to low wave number. Even though this frequency shift is less significant at short wavelength limit and at higher values of wave number/frequency (Fig. 10f), it can be used to construct acoustic diodes.

4.3 2D Fourier transform of the response

After studying the waveform evolution in spatial and wave number domains, we present the contour of 2D Fast Fourier transform (2D-FFT) or 2D power spectrum of the signal in both frequency and wave number domains (see Figs. 11 and 12). Contour plots allow us to reconstruct the dispersion curves, especially inside the pseudo-bandgap. Moreover, these plots can be used to detect the birth of solitary waves based on the shape and distribution of frequency–wave number component. At long wavelength limit, the hardening nonlinear chain does not distort the traveling wave as depicted in Fig. 11a. We note here that the contour plots for the linear signal are exactly the same as the signal plot shown in Fig. 11a, thus confirming that the nonlinear chain has no effect in this zone. However, frequency shift and distortion are observed for nonlinear resonator (ω_{d2}) with hardening nonlinearity (Fig. 11b) and softening nonlinearity (Fig. 11c). It is noteworthy that the frequency shift is more significant and the wave distortion is more severe in the case of softening nonlinearity. To demonstrate the importance of tuning the nonlinear resonator, we present the contour plot for the first resonator in Fig. 11d. It can be observed that the distortion in this case is less significant comparing to the plot in Fig. 11b.

At short wavelength limit, the contour plots for the linear traveling wave are plotted in Fig. 11e. We can

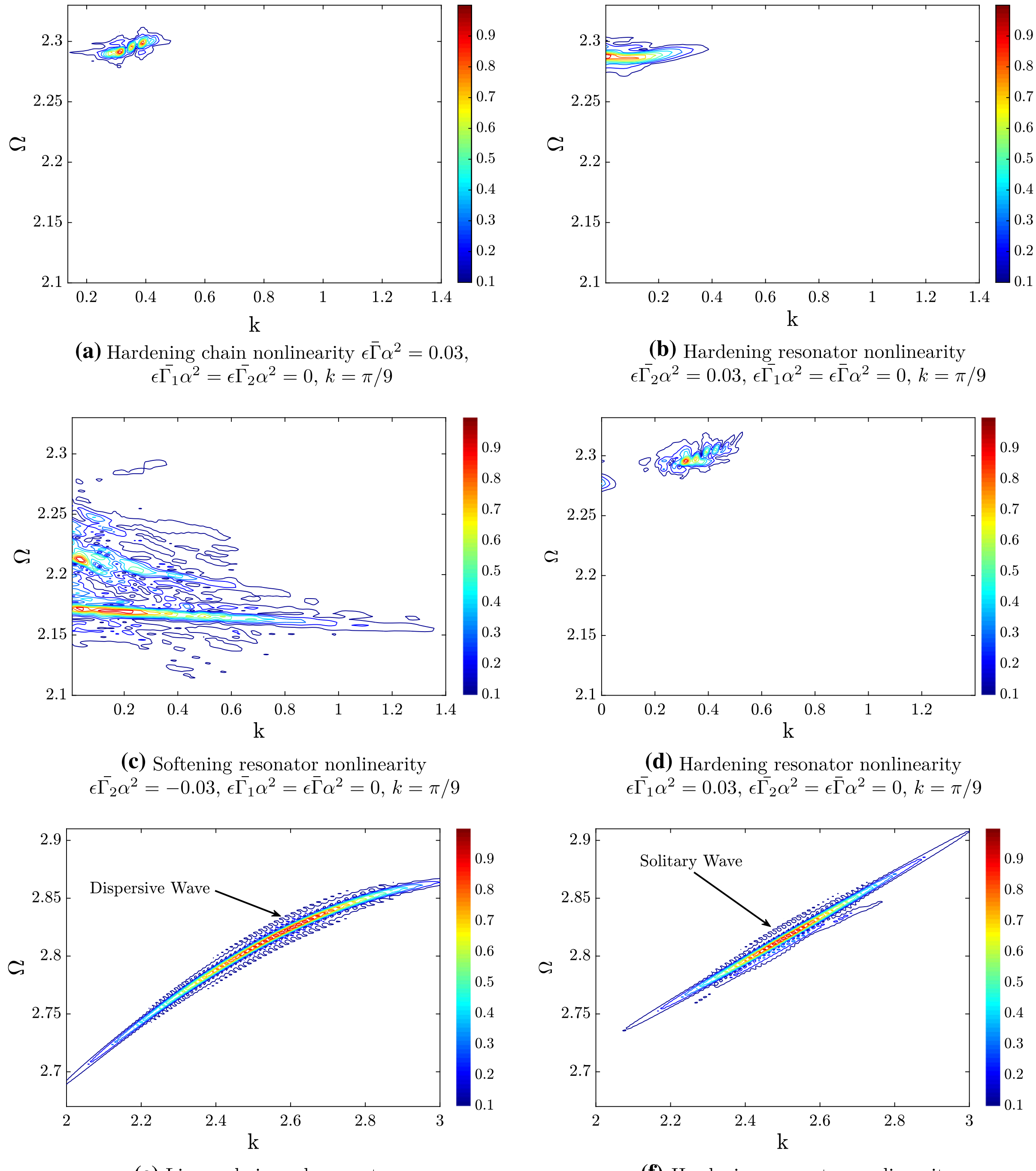

(a) Hardening chain nonlinearity $\epsilon\bar{\Gamma}\alpha^2 = 0.03$, $\epsilon\bar{\Gamma}_1\alpha^2 = \epsilon\bar{\Gamma}_2\alpha^2 = 0$, $k = \pi/9$

(b) Hardening resonator nonlinearity $\epsilon\bar{\Gamma}_2\alpha^2 = 0.03$, $\epsilon\bar{\Gamma}_1\alpha^2 = \epsilon\bar{\Gamma}\alpha^2 = 0$, $k = \pi/9$

(c) Softening resonator nonlinearity $\epsilon\bar{\Gamma}_2\alpha^2 = -0.03$, $\epsilon\bar{\Gamma}_1\alpha^2 = \epsilon\bar{\Gamma}\alpha^2 = 0$, $k = \pi/9$

(d) Hardening resonator nonlinearity $\epsilon\bar{\Gamma}_1\alpha^2 = 0.03$, $\epsilon\bar{\Gamma}_2\alpha^2 = \epsilon\bar{\Gamma}\alpha^2 = 0$, $k = \pi/9$

(e) Linear chain and resonators $\epsilon\bar{\Gamma}_2\alpha^2 = \epsilon\bar{\Gamma}_1\alpha^2 = \epsilon\bar{\Gamma}\alpha^2 = 0$, $k = 7\pi/9$

(f) Hardening resonator nonlinearity $\epsilon\bar{\Gamma}_2\alpha^2 = 0.03$, $\epsilon\bar{\Gamma}_1\alpha^2 = \epsilon\bar{\Gamma}\alpha^2 = 0$, $k = 7\pi/9$

Fig. 11 2D Fourier transform contour of the response for different types and sources of nonlinearities at frequencies in the upper branch of dispersion curve

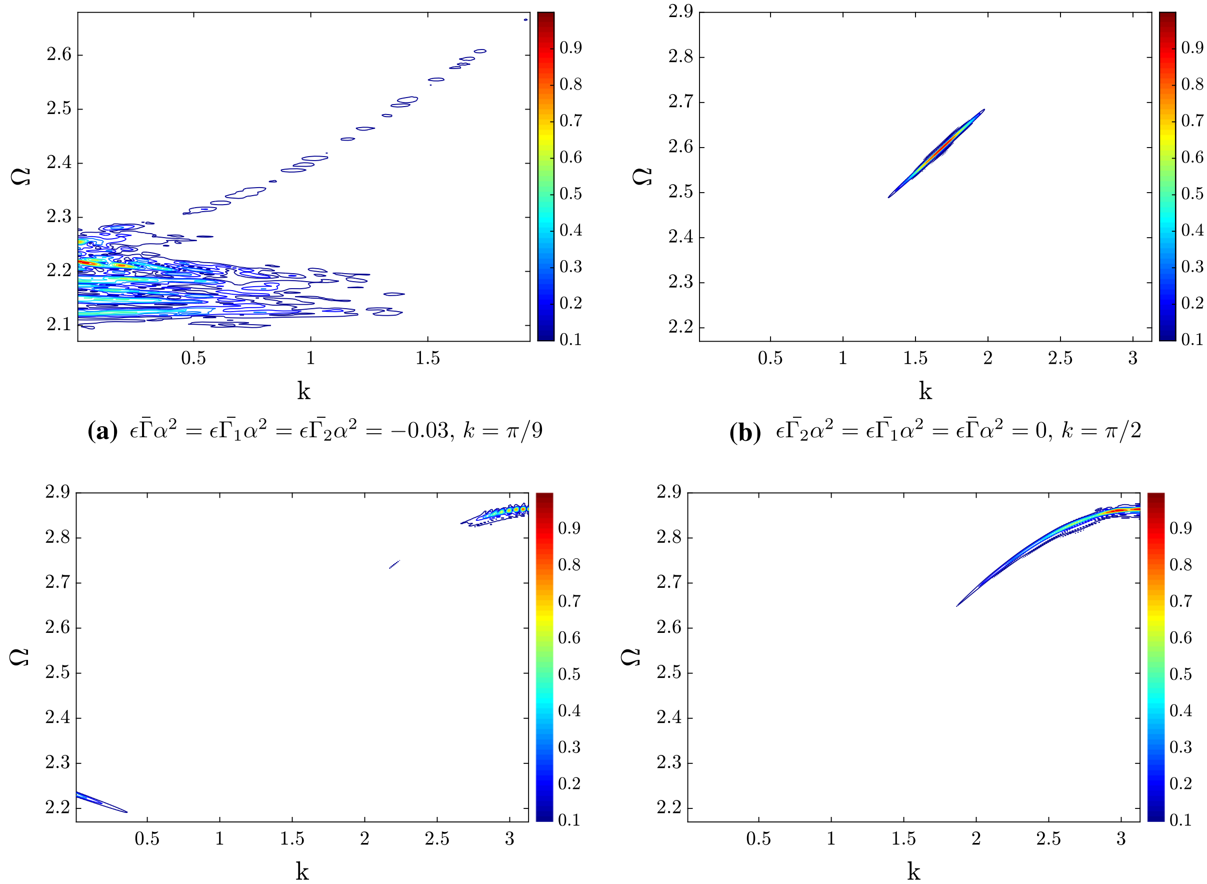

(a) $\epsilon\bar{\Gamma}\alpha^2 = \epsilon\bar{\Gamma}_1\alpha^2 = \epsilon\bar{\Gamma}_2\alpha^2 = -0.03,\ k = \pi/9$ **(b)** $\epsilon\bar{\Gamma}_2\alpha^2 = \epsilon\bar{\Gamma}_1\alpha^2 = \epsilon\bar{\Gamma}\alpha^2 = 0,\ k = \pi/2$

(c) $\epsilon\bar{\Gamma}_2\alpha^2 = \epsilon\bar{\Gamma}_1\alpha^2 = \epsilon\bar{\Gamma}\alpha^2 = -0.03,\ k = \pi/2$ **(d)** $\epsilon\bar{\Gamma}_1\alpha^2 = \epsilon\bar{\Gamma}_2\alpha^2 = \epsilon\bar{\Gamma}\alpha^2 = -0.03,\ k = 7\pi/9$

Fig. 12 2D Fourier transform contour of the response for different types and sources of nonlinearities at frequencies in the upper branch of dispersion curve

observe that the signal density is stretched over a wide range of frequencies. Moreover, the power spectrum of this signal has a variable slope dispersion curve , hence suggesting that the wave is dispersive in this case [25]. However, the stretching of the dispersive wave becomes narrower and the signal tends to become localized when nonlinear hardening resonator is used as depicted in Fig. 11f. We can also observe the presence of some low-amplitude dispersive signals in the surrounding of the localized wave. These dispersive signals were also observed as shown in Sect. 4.1 for hardening nonlinearity in both the resonator and chain. It is obvious here that the localized signal represents a solitary wave since the power spectrum has a linear dispersion curve (constant slope) [25].

Finally, we demonstrate the concept of significant frequency shift by using softening chain and softening resonators at all wavelength limits (Fig. 12). In Fig. 12a, a significant frequency shift is observed at the long wavelength limit. This shift locates the dominant frequency component at frequencies much lower than the predicted frequencies in the linear case (see Fig. 11a for comparison). At medium wavelength limit, the frequency shift is more significant comparing to the other cases as shown in Fig. 12c. The original signal (Fig. 12b) is completely distorted and shifted to frequencies in the maximum and minimum level of the upper dispersion curve. At short wavelength limit (Fig. 12d), a frequency shift can also be observed. Although this shift is less significant comparing to other wavelength limits, the initial frequency bands are clearly shifted to the end of the dispersion curve. Furthermore, the dispersion curve tends to be more nonlinear; thus, the wave is more dispersive [25]. The afore-

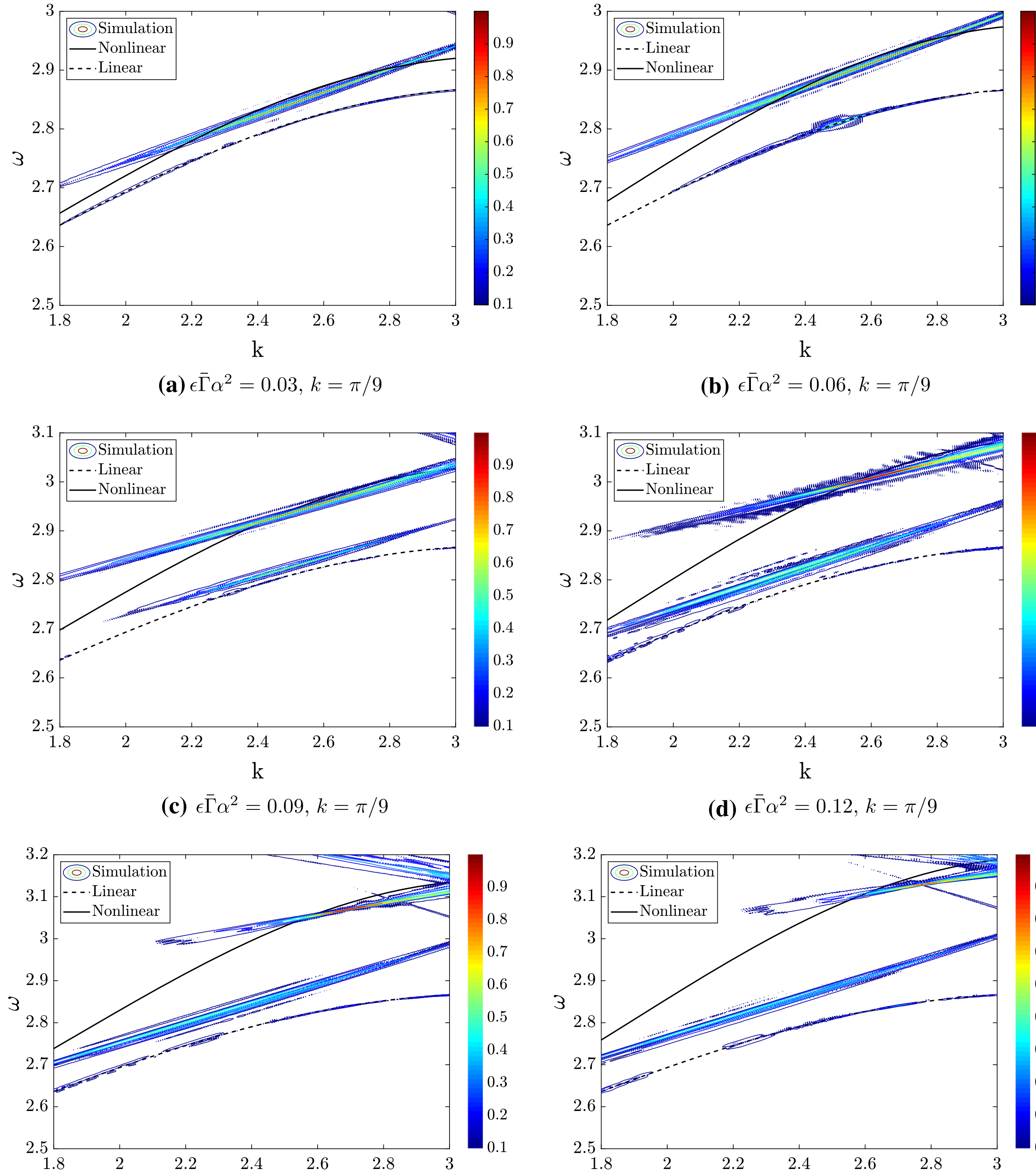

(a) $\epsilon\bar{\Gamma}\alpha^2 = 0.03,\ k = \pi/9$

(b) $\epsilon\bar{\Gamma}\alpha^2 = 0.06,\ k = \pi/9$

(c) $\epsilon\bar{\Gamma}\alpha^2 = 0.09,\ k = \pi/9$

(d) $\epsilon\bar{\Gamma}\alpha^2 = 0.12,\ k = \pi/9$

(e) $\epsilon\bar{\Gamma}\alpha^2 = 0.15,\ k = \pi/9$

(f) $\epsilon\bar{\Gamma}\alpha^2 = 0.18,\ k = \pi/9$

Fig. 13 Comparison between approximate analytical solution and contour plots of 2D-FFT of the numerical simulations for nonlinear chain case

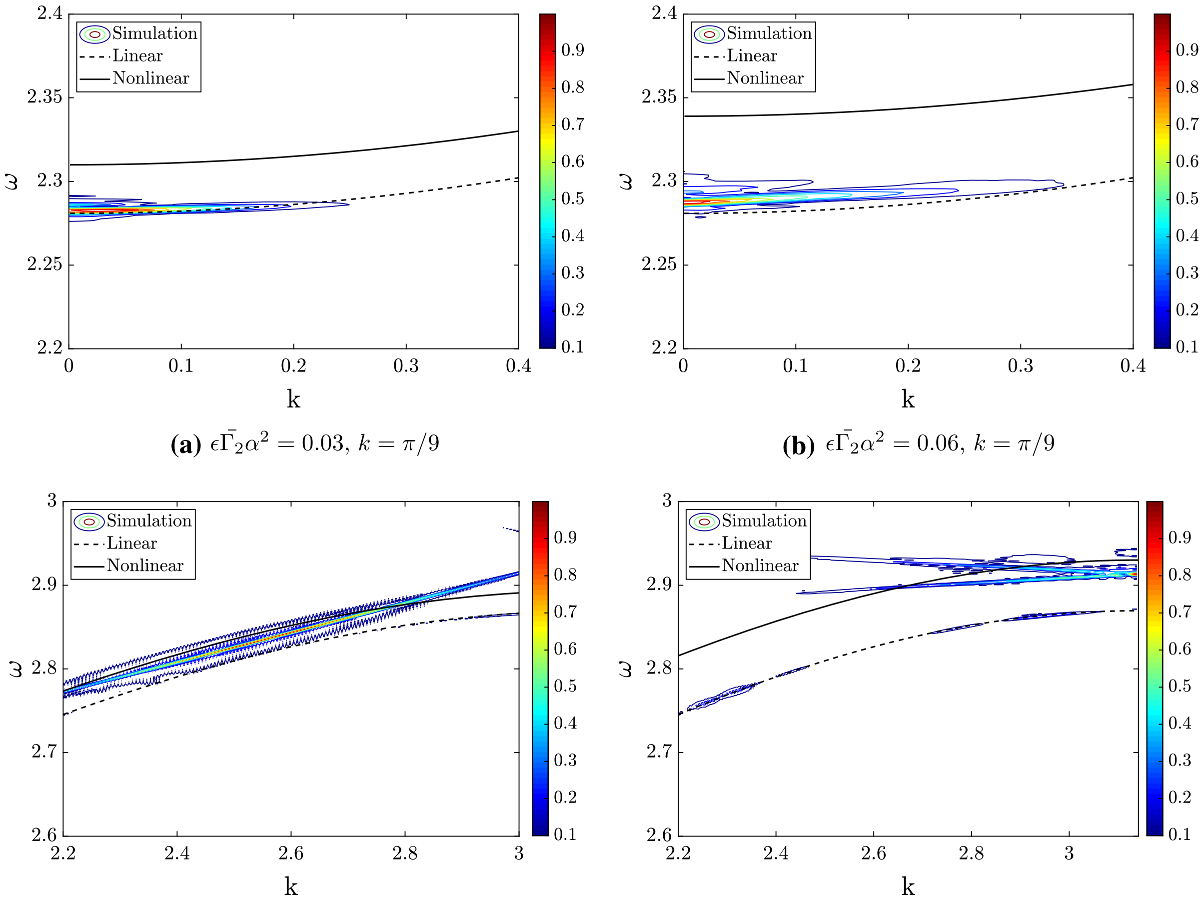

(a) $\epsilon\bar{\Gamma}_2\alpha^2 = 0.03,\ k = \pi/9$

(b) $\epsilon\bar{\Gamma}_2\alpha^2 = 0.06,\ k = \pi/9$

(c) $\epsilon\bar{\Gamma}_2\alpha^2 = 0.06,\ k = 7\pi/9$

(d) $\epsilon\bar{\Gamma}_2\alpha^2 = 0.15,\ k = 7\pi/9$

Fig. 14 Comparison between approximate analytical solution and contour plots of 2D-FFT of the numerical simulations for nonlinear resonator case

mentioned frequency shifts reveal that a wider pseudo-bandgap can be formed by using softening chain and softening resonators. This pseudo-bandgap can be utilized for constructing acoustic diodes with a wide range of operational frequencies.

5 Limitation of the approximate analytical solution by contour plots

After analyzing the spectro-spatial analysis of the wave propagating in a nonlinear metamaterial and showing the possibility of predicting the nonlinear dispersion curves from the contour plots, we now study the limitations of the approximate analytical solution by increasing the strength of nonlinearity. This can be done by comparing the analytical results with their corresponding contour plots.

For the case of nonlinear chain, we compare our solution derived by the method of multiple scales to the dispersion curves obtained by the contour plots of the 2D-FTT of the numerical simulations for different strengths of nonlinearity as shown in Fig. 13. This comparison is done in the short wavelength limit (in the upper optical branch of the dispersion curves) since this region is the most affected by nonlinearity as shown in Sect. 3. For small value of nonlinearity ($\alpha^2\epsilon\Gamma \leq 0.06$), our approximate analytical solution shows a good agreement with the contour plots of the numerical simulations as shown in Fig. 13a, b. It can also be observed that the other wave with linear profile coincides with the linear dispersion curves.

Increasing the nonlinearity further results in an additional weak nonlinear wave, which lies between the linear and nonlinear dispersion curves as shown in Fig. 13c, f. The energy content in this wave increases with the increase in nonlinearity. Yet, Fig. 13c, e indicates that our approximate analytical solution can still predict the upper boundaries of the dispersion curve for ($\alpha^2\epsilon\Gamma \leq 0.015$). Beyond this value ($\alpha^2\epsilon\Gamma \geq 0.15$), we observe that our approximate analytical solution fails to accurately predict the upper boundary of the dispersion curve as shown in Fig. 13f.

As for the case of nonlinear resonators, the comparison of the approximate solution and the 2D-FTT contour plot of the numerical simulation is shown in Fig. 14. Considering frequencies closer to the nonlinear resonator frequency and focusing on the long wavelength limit, Fig. 14a, b shows that our approximate analytical solution cannot accurately predict the dispersion curve of the system even for small values of nonlinearity. However, when considering the region away from the nonlinear resonator frequency and focusing on the short wavelength limit, Fig. 14c, d demonstrates that our approximate analytical solution can accurately predict the nonlinear dispersion curve for small values of nonlinearity. This accuracy vanishes for larger value of nonlinearity ($\epsilon\bar{\Gamma}_2\alpha^2 \geq 0.15$).

6 Conclusion and future work

In this paper, we investigated a nonlinear metamaterial consisting of a nonlinear chain with multiple nonlinear local resonators. Using the method of multiple scales, we obtained explicit expressions for the nonlinear dispersion relations for a nonlinear chain with multiple nonlinear resonators. These expressions were validated by the numerical simulations and results in the literature. The validation indicated that our analytical solution can accurately predict the cutoff frequencies of the dispersion curves and the boundaries of the bandgaps. However, the analytical results failed to predict the behavior of the nonlinear system in region near the frequency of the nonlinear local resonator and the pseudo-bandgap for wave packet input signal simulations. The pseudo-bandgap has a unique feature since a significant frequency shift can be observed inside this zone. Nevertheless, analytical expressions can still reveal the wavelength zones affected by nonlinearity. The nonlinearity only affected the short wavelength limit for the case of nonlinear chain. However, for the case of nonlinear resonators, this nonlinear affected all wavelengths, particularly when the resonator was properly tuned. This observation was consistent with the topological analysis.

In the spectro-spatial analysis, the results showed the existence of solitary wave with hardening nonlinearity and dispersive wave with softening nonlinearity. This wave distortion cannot be observed at long wavelength limit in the nonlinear chain case. However, nonlinear local resonators stretch the wave in this zone with both types of nonlinearities. The amplitude of this dispersive wave was much higher with hardening nonlinearity. This wave distortion depends on the nonlinear resonator frequency and how close it is to the input wave frequency. These observations were also confirmed by spectrograms and contour plots of 2D Fourier transform. For different combinations of nonlinearities, the spectrograms demonstrated significant frequency shift in the medium wavelength limit when the chain and resonator have both hardening nonlinearity. However, this frequency shift can be observed at all wavelength limits when we change the nonlinearity type to softening. Finally, the contour plots showed a wide pseudo-bandgap demonstrating a significant frequency shift at all wavelength limits. The implication is that this pseudo-bandgap can be utilized to design and construct acoustic diodes with a wide range of operation frequencies. For future work, the authors plan to experimentally demonstrate the benefits of the revealed phenomena.

Acknowledgements This work was supported by the start-up grant provided by the Department of Mechanical Engineering at Virginia Tech.

Compliance with ethical standards

Conflict of interest The authors declare that they have no conflict of interest.

References

1. Hussein, Mahmoud I., Leamy, Michael J, Ruzzene, Massimo: Dynamics of phononic materials and structures: historical origins, recent progress, and future outlook. Appl. Mech. Rev. **66**(4), 040802 (2014)
2. Cai, Wenshan, Shalaev, Vladimir M: Optical Metamaterials, Volume 10. Springer, Berlin (2010)
3. Achaoui, Younes, Laude, Vincent, Benchabane, Sarah, Khelif, Abdelkrim: Local resonances in phononic crystals and in

random arrangements of pillars on a surface. J. Appl. Phys. **114**(10), 104503 (2013)
4. Bertoldi, Katia, Vitelli, Vincenzo, Christensen, Johan, van Hecke, Martin: Flexible mechanical metamaterials. Nat. Rev. Mater. **2**(11), 17066 (2017)
5. Sigalas, Michael M., Economou, Eleftherios N.: Elastic and acoustic wave band structure. J. Sound Vib. **158**, 377–382 (1992)
6. Sigalas, M., Economou, Eleftherios N.: Band structure of elastic waves in two dimensional systems. Solid State Commun. **86**(3), 141–143 (1993)
7. Kushwaha, Manvir S., Halevi, Peter, Dobrzynski, Leonard, Djafari-Rouhani, Bahram: Acoustic band structure of periodic elastic composites. Phys. Rev. Lett. **71**(13), 2022 (1993)
8. Kushwaha, Manvir S., Halevi, P., Martinez, G., Dobrzynski, Leonard, Djafari-Rouhani, Bahram: Theory of acoustic band structure of periodic elastic composites. Phys. Rev. B **49**(4), 2313 (1994)
9. Vasseur, J.O., Djafari-Rouhani, B., Dobrzynski, L., Kushwaha, M.S., Halevi, P.: Complete acoustic band gaps in periodic fibre reinforced composite materials: the carbon/epoxy composite and some metallic systems. J. Phys. Condens. Matter **6**(42), 8759 (1994)
10. Kushwaha, Manvir S.: Classical band structure of periodic elastic composites. Int. J. Modern Phys. B **10**(09), 977–1094 (1996)
11. Liu, Zhengyou, Zhang, Xixiang, Mao, Yiwei, Zhu, Y.Y., Yang, Zhiyu, Chan, Che Ting, Sheng, Ping: Locally resonant sonic materials. Science **289**(5485), 1734–1736 (2000)
12. Liu, Liao, Hussein, Mahmoud I: Wave motion in periodic flexural beams and characterization of the transition between Bragg scattering and local resonance. J. Appl. Mech. **79**(1), 011003 (2012)
13. Huang, G.L., Sun, C.T.: Band gaps in a multiresonator acoustic metamaterial. J. Vib. Acoust. **132**(3), 031003 (2010)
14. Zhu, R., Liu, X.N., Hu, G.K., Sun, C.T., Huang, G.L.: A chiral elastic metamaterial beam for broadband vibration suppression. J. Sound Vib. **333**(10), 2759–2773 (2014)
15. Kivshar, Yuri S., Flytzanis, Nikos: Gap solitons in diatomic lattices. Phys. Rev. A **46**(12), 7972 (1992)
16. Nadkarni, Neel, Daraio, Chiara, Kochmann, Dennis M: Dynamics of periodic mechanical structures containing bistable elastic elements: from elastic to solitary wave propagation. Phys. Rev. E **90**(2), 023204 (2014)
17. Liang, Bin, Yuan, Bo, Cheng, Jian-chun: Acoustic diode: rectification of acoustic energy flux in one-dimensional systems. Phys. Rev. Lett. **103**(10), 104301 (2009)
18. Manimala, James M., Sun, C.T.: Numerical investigation of amplitude-dependent dynamic response in acoustic metamaterials with nonlinear oscillators. J. Acoust. Soc. Am. **139**(6), 3365–3372 (2016)
19. Nayfeh, Ali H.: Introduction to Perturbation Techniques. Wiley, Hoboken (2011)
20. Nayfeh, Ali H., Mook, Dean T.: Nonlinear Oscillations. Wiley, Hoboken (2008)
21. Narisetti, Raj K., Leamy, Michael J., Ruzzene, Massimo: A perturbation approach for predicting wave propagation in one-dimensional nonlinear periodic structures. J. Vib. Acoust. **132**(3), 031001 (2010)
22. Manktelow, Kevin, Leamy, Michael J., Ruzzene, Massimo: Multiple scales analysis of wave-wave interactions in a cubically nonlinear monoatomic chain. Nonlinear Dyn. **63**(1–2), 193–203 (2011)
23. Lazarov, Boyan Stefanov, Jensen, Jakob Søndergaard: Low-frequency band gaps in chains with attached non-linear oscillators. Int. J. Non-Linear Mech. **42**(10), 1186–1193 (2007)
24. Khajehtourian, Romik, Hussein, Mahmoud I.: Dispersion characteristics of a nonlinear elastic metamaterial. AIP Adv. **4**(12), 124308 (2014)
25. Hussein, M.I., Khajehtourian, R.: Nonlinear Bloch waves and balance between hardening and softening dispersion. Proc. R. Soc. A Math. Phys. Eng. Sci. **474**(2217), 20180173 (2018)
26. Liang, B., Guo, X.S., Tu, J., Zhang, D., Cheng, J.C.: An acoustic rectifier. Nat. Mater. **9**(12), 989 (2010)
27. Xue-Feng Li, Xu, Ni, Liang Feng, Ming-Hui, Lu, He, Cheng, Chen, Yan-Feng: Tunable unidirectional sound propagation through a sonic-crystal-based acoustic diode. Phys. Rev. Lett. **106**(8), 084301 (2011)
28. Ma, Chu, Parker, Robert G., Yellen, Benjamin B.: Optimization of an acoustic rectifier for uni-directional wave propagation in periodic mass-spring lattices. J. Sound Vib. **332**(20), 4876–4894 (2013)
29. Boechler, Neil, Theocharis, Georgios, Daraio, C.: Bifurcation-based acoustic switching and rectification. Nat. Mater. **10**(9), 665 (2011)
30. Moore, Keegan J., Bunyan, Jonathan, Tawfick, Sameh, Gendelman, Oleg V, Li, Shuangbao, Leamy, Michael, Vakakis, Alexander F: Nonreciprocity in the dynamics of coupled oscillators with nonlinearity, asymmetry, and scale hierarchy. Phys. Rev. E **97**(1), 012219 (2018)
31. Ganesh, R., Gonella, Stefano: Spectro-spatial wave features as detectors and classifiers of nonlinearity in periodic chains. Wave Motion **50**(4), 821–835 (2013)
32. Zhou, W.J., Li, X.P., Wang, Y.S., Chen, W.Q., Huang, G.L.: Spectro-spatial analysis of wave packet propagation in nonlinear acoustic metamaterials. J. Sound Vib. **413**, 250–269 (2018)
33. Bukhari, M.A., Barry, O.R.: Nonlinear metamaterials with multiple local mechanical resonators: Analytical and numerical analyses. In: NODYCON 2019 The First International Nonlinear Dynamics Conference. (Accepted) (2019)
34. Bukhari, M., Barry, O.: On the spectro-spatial wave features in nonlinear metamaterials with multiple local resonators. In: ASME 2018 International Design Engineering Technical Conferences and Computers and Information in Engineering Conference. American Society of Mechanical Engineers (2019)